# Investigation of the Use of Forced Vibrations as a Means to Estimate the Condition of Bridge Deck Systems

J. E. Stephens, Prof. of Civil Engineering

August 1979

Project 72-2 JHR 79-129

TABLE OF CONTENTS

Acknowledgements:

The computer-program portion of this study was developed by Claude Johnson and John Risley. The study has been conducted as a joint project between the Civil Engineering Department of the University of Connecticut and the Office of Research of the Connecticut Department of Transportation.

## List of Tables



## List of Figures

## Introduction

Shortly after the Point Pleasant, West Virginia bridge collapse, the question of how to monitor the conditions of Connecticut's many bridges was raised by the Commissioner. Thorough inspection can reveal most types of deterioration, but certain developing troubles can be determined only by tests. The best example of the latter is fatigue. After repeated high stresses the ultimate strengths of both steel and conrete are reduced. The rate of change of the ultimate strength increases as the level of repeated stress increases. The load/stress/material strength ratio varies from truss member to truss member or from point to point in a beam or slab. Thus, the service life of each portion of a structure is different. In some instances, deformation of an overloaded member may transfer excess load to other members, staving off serious failure. In other instances, work hardening may increase the modulus of elasticity causing the member to piek up more load and hasten failure. The general relationships portrayed in figure #1 apply at every point within a structure. Most structures are exposed to ever-increasing wheel loads. In fact, the loads are applied with a degree of impact. With time, increased roughness increases the impact load for a constant axle load.

In structural work, the load cycles do not start or end at zero due to the dead load. Fatigue should be related to the range of loading change. For example, cycling from 60% of static strength to 70% should have a different fatigue effect than from 70% to 80%. This indicates that modern structures designed to utilize more fully the strength of materials may fatigue faster than older proportionately heavier structures.

Although loadings are stated in terms of the number of vehicles, fatigue cycles for much of a structure are related to the number of vibrations occurring. As the frequency of structural vibration increases and the mass decreases, lighter structures may accumulate fatigue cycles more rapidly than

similar heavy spans.

These complex interactions make inspection for fatigue anything but precise. As all portions of a bridge span work together to carry a load, measurement of total structure stiffness or deflection should reflect the effect of any defective material.

The Gold Star bridge from New London to Groton was proposed as a site where measurements could be made under some form of controlled load. The problem of establishing a fixed reference for this high-level structure and of controlling traffic during testing made this site impractical. Constant small failures of bridge-deck surfaces capped by large-area failures in the Turnpike Housatonic River Bridge resulted in changing the thrust of the study to concrete decks. The problem appeared universal with several states pointing out that bituminous concrete overlays had compounded the problem by concealing further deterioration. Apparently no factual information concerning current status of deck concrete or estimated future maintenance schedules or costs were available in most states. Repairs were made when the surface condition had deteriorated to a degree objectionable to the driver.

Any prodedure to be used routinely for condition surveys must not unduly interfere with traffic. Recognizing the advantages of utilizing proven and time tested equipment, several systems of evaluation were reviewed. In the middle fifties, sound waves were used to determine the degree of concrete damage caused by alkali reaction. The equipment evolved into the sonometer now used widely for determining the sonic modulus of concrete. In its present form, a transducer placed against one end of a prismatic sample of concrete transmits a frequency into the material. A second transducer at the opposite end of the sample picks up this signal, Fig. 2. The frequency of the signal is varied and resonance determined. Given several similarly shaped specimens, the resonant frequency can be used to rank the specimens as to quality of

concrete. Numerical values of concrete strength must be determined by comparisons with the results of compression tests of similar concrete. When used as a measure of condition of real-life concrete, the transducers may have to be located on the same surface of the concrete, and the available transducer power may not be adequate to overcome dissipation into the mass. Determination of resonance is then difficult or impossible. The rate of propagation of sound waves through concrete is also a measure of quality or condition. Regrettably, for modest sections and short distances, the precision of timing needed is beyond that of the equipment.

Any sonic procedure would require a delay of traffic to avoid spurious vibration which would mask the small signal used. The reinforcing rod in the deteriorated area would give an excellent path for the signal and would probably conceal any change due to a decrease in concrete quality. This procedure can not be considered suitable.

The use of a more powerful signal would reduce the pickup and recording problems. Two devices using powerful signals or loadings are available. Both the Dynaflec$^{R}$ and the Roadrater$^{R}$ apply a large vibrational or cyclic loading to the pavement and measure the amplitude of the wave at various distances from the point of load. The Dynaflec utilizes rolling transducers composed of small steel rollers to transmit a cyclic load to, and receive vibrations from, the pavement. The surface condition of many roads jostle the rollers, and result in substantial noise in the instrumentation. However, the controlled load cycling produces a constant frequency signal which can be sorted out from the random noise. To control the noise, the rate of travel is usually limited to 10 mph. In contrast, the Roadrater transport vehicle is stationary for the duration of each test. The load is placed on the pavement and vibrated. As the load is lowered to the pavement, four accelerometers are positioned on the pavement, at the center of the load, 1, 2 and 3 feet ahead. As a Roadrater

was based on Long Island, it was selected for the tests. The stop-test-move sequence takes approximately one minute and, though an inconvenience to traffic, was acceptable. Traffic, other than that on the span under test, need not be stopped as the use of a load of 500 pounds gave a signal strong enough to overcome the noise from all but the largest trucks moving in the vicinity.

## Procedure

A number of structures were selected for testing. Precast concrete box girders typical of the 1955 flood replacements, composite decks, and bituminous wearing surfaces were included. Table I lists those which were tested in the first day of testing in 1970. The general configuration of the Roadrater is shown in Figure 3. In 1970 the ram weight was 850#. For each bridge, the location of the girders was laid out on the deck. One pass was made along the deck directly over a girder, with tests made at the mid span and at six feet from each end. A second pass was made midway between two girders. As interest at the time was focused on rate of deterioration, these points were assumed as typical of each deck and would be tested again later for comparison.

The Roadrater consists of a double acting hydraulic ram with two loading pads on the lower end, a hydraulic pumping system, an air suspension for the ram, a programmable control unit and a vibration-sensing system all mounted on the front of a small van. When activated, the ram loads the pavement sinusoidally (Figure 4) with the magnitude and frequency of the load set by the operator. When in operation, the static load of the ram is increased by momentum so that the dynamic load actually induced is somewhat greater than the weight of the ram.

One vibration sensor (accelerometer) is located between the loading pads and others can be added at intervals forward of the pads. In 1970 and again in 1973, two sensors were used, one at the center of the contact pads

and one located one foot ahead. The amplitude of vibration at both sensor locations was recorded in inches x $10^{-5}$. The values recorded in 1970 and 1973 were similar at some locations and sharply different at others. In principle, two identically dimensioned structures under identical loads should deflect inversely with the stiffness. Similarly, under dynamic loading, the greater the dynamic stiffness the less the dynamic deflection. The increase in concrete quality due to age from, for example, the 15th to the 18th year of service, should be far less than the decrease in quality over the same period due to fatigue and weathering, resulting in a decrease in dynamic stiffness, which should be indicated by increased deflection. The expected general increases in vibration deflection were not found. Closer study revealed that the Roadrater had been altered during the interval between the two test series and the minimum load was now greater than that used before. As a consequence, the very simple comparison anticipated could not be made.

Certain characteristics of the vibrations could be readily seen from the data. The resonant frequency of the short spans (30 ft) was within a few cycles of the test-load frequency and the relatively small load caused substantial vibrational deflection. The magnitude of vibration along one short-span girder had been so great in 1970 that measurements were made at 1-1/2 ft. intervals, Figure 5. When repeated in 1973, the vibration had the same shape but the magnitude was smaller. This decrease, under increased load, is explained by a shift in loading frequency away from resonance. The difference in vibration magnitude sensed at the load center and one foot away was small. In Figures 5 and 6 the maximum vibration occurred slightly to one side of the span center. This discrepancy is explained by the weight of the van being to one side of the loaded area. Most of the curves plotted revealed this minor end to end nonsymmetry.

For longer spans (60 ft.), the middle value was often smaller than the end vibrations, Figure 6. These spans vibrated in the second mode and more test points would have shown one point nearly stationary and maxiumum at the quarter points. Again, the weight of the van displaced the curve to the left. The longer spans had a resonant frequency below that of the test load and the maximum vibration amplitude was smaller than that of the short spans. Figures 5 and 6 imply that the bulk of the vibration measured is the longitudinal vibration of the girders. Three points in the length of a span do not provide sufficient information for delineation of a second-order vibration superimposed on the prime vibration. However, for the trial at spacings of 1-1/2 feet, there is no indication of higher modes of vibration. Transverse vibration might reflect variations in concrete, but sufficient points were not tested to make transverse plots possible. No pass over any of the structures revealed vibration magnitudes that could be identified as resulting from poor or deteriorating concrete.

It was concluded that the three-point testing would reveal only extensive areas of low-strength concrete located in a manner such as to affect the flexure strength of the girders. The procedure as employed does not have sufficient sensitivity to be useful in determining development of deterioration until the problem is serious.

High-speed computers have made possible solution of dynamic equations for the displacement of a vibrating structure after a selected period of time. Vibration magnitudes found by the Roadrater should approximate those so computed. The computations use as input the physical characteristics of the materials, the structure dimensions and the loading. If the vibration magnitudes measured do not agree with those computed, then a better estimate of the concrete quality can be obtained by finding the modulus of elasticity,

which when used in the computations results in the measured dynamic deflections.

STRUDL-II (Structural Design Language - Version II) was mounted on the University IBM 730 computer. This program was developed by the MIT Civil Engineering Department and includes dynamic analysis of multi-degree-of-freedom systems. The STRUDL dynamic analysis program is executed in three phases. In the first phase, the structure is considered to be idealized such that the dynamic equilibrium equation is of the matrix form:

$$M\ddot{x} + C\dot{x} + Kx = F(t) \qquad \text{(Eq. 1)}$$

where: $M$ = system mass matrix

$C$ = system damping matrix

$K$ = system stiffness matrix

$x, \dot{x}, \ddot{x}$ = time-dependent displacement, velocity and acceleration vectors, respectively

$F(t)$ = vector forcing function

This phase of the program computes the mass and stiffness matrices utilizing the structure geometry, the connectivity of the parts and the material properties.

In the second phase, the matrices are introduced into equation one and this equation transformed into a characteristic real eigenvalue problem. The results of the eigenvalue problem are the physical system frequencies and model shapes. For a given structure, each of the normal modes of vibration has an explicit frequency. Using a flat plate as an example, Figure 7 shows the first six normal vibration modes in the order of increasing frequency.

The third phase combines the loading function with each normal mode and frequency to compute the dynamic displacement for each mode at selected times. The displacement at the selected times is then the summation of the displace-

ments contributed by each mode.

As the STRUDL program is very time consuming, it is expensive to run. As a result, it was decided to limit the future tests on structures to two bridges. State bridge #1200 at study site #6 carries Sarella Road traffic over I-84. This four-span structure is approximately symmetrical about the center pier, Figures 8-9. State bridge #1202 at study site #7 carries Old Hawleyville Road over I-84. The structure is similar to that of Figures 8-9.

For STRUDL analysis, the deck must be divided into elements. Selection of elements is critical as deflections are found at corners or nodes. Girders must fall along lines connecting nodes. The size of element determines the accuracy of the computed deflections. The program can accommodate only a limited number of nodes or elements, and performed well only with triangular elements. The element configurations selected are shown in Figures 10 and 11. Each node (corner of element) had three degrees of freedom: translation vertically, rotation about a longitudinal axis parallel to the girders, and rotation about a transverse axis perpendicular to the girders. As the deflections would be computed at the nodes only, the general plan of nodes was transferred to the bridge deck by locating the girders and centerline of bearing on each span deck. All structures ran S-N, and for simplicity, the spans were designed A, B, C, and D from south to north. The longitudinal lines were marked with letters, starting with A in the east gutter. The transverse lines were given numbers. For the STRUDL program, the overhang of 3' at the abutments was applied as a static load. Short overhangs were ignored. The test point locations and identities are shown in Figures 12 and 13. The grid was considered simply supported along the centerline of bearing. The steel girders were considered to act compositely with the concrete deck. Moments of inertia were computed for composite girders using dimensional limits

in accord with the American Concrete Institute Handbook. Material properties assumed were those frequently used in structural analyses: Poisson's ratio: for concrete 0.15, for steel 0.30; Modulus of Rigidity G = 12,000 ksi; density: for concrete 150 pcf and for steel 490 pcf; Modulus of Elasticity, E: for steel 29,000 ksi, and for concrete

$$E_c = 33\ w^{3/2}\ \sqrt{f'_c}$$

where w = unit weight of reinforced concrete

$f'_c$ = allowable stress of the mix

The additional mass developed from the diaphragms, stiffness of the girders, sidewalks and railings were distributed proportionately to the nearest nodes as additional weight. The analytical loading most nearly representing the experimental loading was a sinusoidal in nature with an amplitude of 1,000 pounds and a frequency of 25 cycle per second. The program output was the acceleration, velocity, and displacement of each mode at time intervals of 0.01 seconds from 0 to 2 minutes.

For most spans, the deck and girder system was roughly symmetrical. For every configuration of test-load vibration sensing there is a second configuration rotated 180° about the geometric center from the first which should give the same result. For example, in Figure 14 placing the test load at G or at C should give similar results. One accelerometer was used on the end of a length of cable to permit measurements remote from the loading. The symmetrical approach remains valid for measurements made remote from the loading such as loading at G measuring at C compared to loading at C measuring at G. The plotted data will be limited to these two configurations designated Measured Where Loaded (MWL) and Measured Symmetrically Opposite Load (MSOL).

Results

Figures 15-17 present data obtained for the short end spans. In Figure 15, J5 corresponds to A1 and so the entire b portion of the curve has been reversed for ease of comparison. All four curves show a single mode of vibration. The nonsymmetry from end to end is due to the position of the weight of the van. When loading A2 the van weight is near A1 and does little to damp the vibration. When loading A4 the van weight approximates A3 and sharply damps the wave.

The skew angle also affects the shape of the longitudinal vibration magnitude curve. Considering only two girders, a large amplitude at the center of one tends to increase the amplitude of the deflection of the other at a point opposite. In Figure 18, deflections at a and c increase those at b and d. This effect is additive to the van weight at some positions and subtractive at others. In Figure 15, Curve 1 follows very closely curve 4 and seems to verify the approach. However, Curve 2 is sharply below curve 3 with no explanation apparent.

Figure 16 represents the far-end span, which in length is very close to span A. Again curves 1 and 4 are very similar. As the frequency of loading approaches the resonant frequency of the short spans, minor changes in span length, which change the span resonant frequency, can cause large changes in vibration magnitude. Curves 2 and 3 as in Figure 15 are sharply different; however, for this span, the reverse direction J24 - J20 is the smaller. As this reversal corresponds to the change of overhang from near to far end, this difference in magnitude appears due to the overhang beyond the centerline of bearing.

Non-girder rows A and J were adjacent to the curbs and walks which provide additional stiffness. A similar procedure was applied to non-girder row G and girder row H, which were further from the curbs. The data is presented in Figures 17 and b in which curves 2 and 3 are similar, but 1 and

4 differ substantially. Comparisons amongst curves of Figures 15 to 17 show two distinct groups based on amplitude at mid span. Plotting the mid-point amplitudes across the girders point to two different modes of cross vibration. Span A with a high value at G probably vibrates in the first mode, and span D with the highest value at H in the second mode (Fig. 21).

The end spans A and D of the structure at site 6 were tested along girder rows B and F (Figs. 19 and 20). The length of the end spans at site 7 was 31 feet. At site 6, the south span is 23.5 feet and the north span 37 feet. All the spans in this range of length vibrated in the first mode. The magnitude of maximum midspan vibration of girder traverses is directly related to length (Fig. 22).

The mode of vibration for longer spans becomes very complex. Amplitudes must be compared to adjacent points both longitudinally and transversely. Diagrams of equal amplitude become the most vivid representation. The position of the loading vehicle alters the vibration. With the load in a fixed position the amplitude was found at all points. Figure 23 shows the amplitude of vibration throughout span B at site 6 with the load centered on the structure. Longitudinally, the structure is vibrating in the first mode, but transversely a higher mode is occurring. The amplitude of the single mode is approximately $75 \times 10^{-5}$ inches and that of the transverse wave $225 \times 10^{-5}$. There appears to be no anomaly in the deck as the pattern is symmetrical.

Span C of site 6 is represented in Figure 24. The pattern is similar with the change in magnitude attributable to the change in span length.

In use, the load moves on the deck. Placing the load off center should distort the symmetric pattern of Figures 23 and 24. A few points were attempted with nonsymmetric loading. Figures 25 and 26 are for two such loads, which while nonsymmetric are similar to each other. The vibration magnitude patterns

show the stiffening effect of the curb-railing assembly as in both cases maximum amplitudes occur near the center of the structure width. The greatest amplitude does not occur at the load. That the general mode of vibration is more eleaborate than a simple first mode is evidenced by high magnitudes near the far end and to the far side. At the time of the field measurements, it was not deemed necessary to cover the entire deck in order to verify the similarity in patterns represented by Figures 25 and 26. It is interesting to note that very high vibration amplitudes are shown at small isolated areas well removed from the loaded areas. As the curvature and stresses in the deck at these sharply defined areas must be the extreme for the loadings, fatigue may well be equally spotty. The first impression is that of concentrations due to variable quality of material. However, the probability of symmetrically located low-quality material is low, and the vibration variation must be attributed to the structural shapes.

Comparisons have been attempted between the measured and computer projected vibration magnitudes. Figure 27 presents the measured values for span D site 6 and Figure 28 comprises the computed values at the same points under the same loading. The differences in patterns are not great. The only truly significant factor being the difference in magnitude at midspan toward either edge. The computed deflections are approximately half of those measured. The properties assumed for steel must be correct as deflections at the center due to longitudinal vibration are the same. The propagation of deflection transversely is related to the stiffness of the deck concrete. As the measured vibration is greater toward either edge, the concrete appears less stiff than assumed for the computer program.

In a similar way Figure 29 of computed magnitudes for span B site 6 compares well to Figure 23. Again the measured edge vibrations are approximately

double those computed. For the C span at site 6, compare Figure 30 to Figure 24. Again the edge vibrations measured are well above those computed. As the differences are universal for all spans considered, it is more probable that some material property was selected incorrectly for the computer solution than that the concrete is locally poor.

Magnitudes for the nonsymmetric loading agree well. The localized high magnitude areas noted in Figures 25 and 26 are present in the graph of computed deflections (Fig. 31). As the magnitudes are similar, the factor causing the above-mentioned difference in magnitude may be more properly attributed to the manner in which the curb and railings were introduced into the computations.

It is apparent from Figures 23 to 32 that the instrumentation of the Roadrater does sense closely the magnitudes of the dynamic load induced vibrations. However, no indication can be found that the system has merit for the original purpose of the study. The original assumption that vibration magnitude was influenced by material quality to the degree that such differences could be identified has not been proven. No anomalies have appeared in the experimental data. The theoretical analysis has given results compatable with the experimental measurements. The one condition under which the results might be construed so as an indication of poor material would be if all of the deck material was of poor quality.

A major reason for selecting the Roadrater for this study was the speed of operation and minimum interference with traffic. As the work progressed and measurements became necessary at a large number of points, these advantages faded away. In the final configuration, the machine occupied one position on the spans and the sensor roved over the entire deck. The interconnecting cable constantly blocked some portion of the roadway requiring closing of one or more lanes. Such a procedure on more heavily traveled spans would cause

serious dislocations of traffic.

The complexity of the cross-sections combined with the skew angles, varying span length, varying overhang at bearings, differences in curb-railing treatments, etc. overshadowed any differences due to material. It is encouraging that the experimental data confirms the computed dynamic deflections found by use of the ICES structural package.

## Conclusions

1. The bridge decks tested in detail show no indication of faculty concrete.

2. The dynamic deformations measured follow a distribution much like that predicted by STRUDL.

3. The equipment is not well suited to locating faculty material in bridge decks.

4. Any effect on the vibration amplitudes from small areas of faulty concrete is superimposed on the larger amplitudes of the normal response of the span.

5. Further attempts to measure deck quality by this equipment are not justified at this time.

## Appendix

## References


1. Van der Poel, C., Dynamic Testing of Road Construction, Journal of Applied Chemistry, Vol. 1, Part 7, July 1951, pp 281-290.

2. Lytton, R. L. Mahoney, J. P., Moore, W. M., Pavement Evaluation: Phase 1. Pavement Evalutaion Equipment, Federal Highway Administration, Offices of Research and Development, Report No. FHWA-RD-75-78, March 1975, p 188.

3. Bhajandas, A. C., Cumberledge, G., Hoffman, G. L., Flexible Pavement Evaluation and Rehabilitation, Transportation Engineering Journal of ASCE, Vol. 103, No. TE 1, January 1977, pp 75-85.

4. Knoll, W. D., Levy, S., Response of Accelermoters to Transient Accelerations, Journal of Research of the National Bureau of Standards, Vol. 45, No. 4, October 1950.

5. Clough, R. W., Penzien, J., Dynamics of Structures, McGraw-Hill, 1975, pp 62-64.

6. Connor, J. J., Ferrante, A. J., Flachsbart, B. B., Hall, J. E., Logcher, R. D., Nelson, M. F., Power, C. M., Wells, R. A., ICES STRUDL-II The Structural Design Language Engineering User's Manual, Structures Division and Civil Engineering Systems Laboratory, Department of Civil Engineering, Massachusetts Institute of Technology, Research Report R68-91, Vol. 1, First Edition, Nov. 1968.

7. Connor, J. J., Logcher, R. D., Nelson, M. F., ICES STRUDL-II The Structural Design Language Engineering User's Manual, Structures Division and Civil Engineering Systems Laboratory, Department of Civil Engineering, Massachusetts Institute of Technology, Research Report R70-77, Vol. II, Second Edition, June 1972, pp 52-211.

8. Wilkinson, J. H., The Algebraic Eigenvalue Problem, Clarendon Press, Oxford, 1965.

9. Connor, J. J., Logcher, R. D., Nelson, M. F., ICES STRUDL-II The Structural Design Language Engineering User's Manual, Structures Division and Civil Engineering Systems Laboratory, Department of Civil Engineering, Massachusetts Institute of Technology, Research Report R70-77, Vol. II, Second Edition, June 1972, p 177.

10. Cheung, Y. K., Zienkiewicz, O. C., The Finite Element Method, McGraw-Hill, 1967.

11. Connor, J. J., Will, G., Computer Aided Teaching of the Finite Element Displacement Method, Department of Civil Engineering, Massachusetts Institute of Technology, Report 69-23, February 1969.

12. Connor, J. J., Logcher, R. D., Nelson, M. F., ICES STRUDL-II The Structural Design Language Engineering User's Manual, Structures Division and Civil Engineering Systems Laboratory, Department of Civil Engineering, Massachusetts Institute of Technology, Research Report R70-77, Vol. II, Second Edition June 1972, p 53.

13. Gilkey, C. H., Jones, T. J., Evaluation of STRUDL-II Dynamic Analysis Capabilities, Combustion Engineering, Inc., June 1973.

14. Risley, John F., A Method of Investigating Bridge Deck Quality Through Dynamic Analysis and Appropriate Testing Comparison, Master's Thesis, University of Connecticut, June 1977.

| SITE NUMBER | CONNDOT BRIDGE NUMBER | ROUTE NUMBER | LOCATION |
|---|---|---|---|
| 1 | 533 | US 7 | Wilton |
| 2 | 536 | US 7 | Ridgefield |
| 3 | 537 | US 7 | Ridgefield |
| 4 | 550 | US 7 | Danbury<br>North Bound Lane at<br>I-84 Interchange |
| 5 | 551 | US 7 | Danbury<br>South Bound Lane at<br>I-84 Interchange |
| 6 | 1200 | I-84 | Bethel<br>Garella Road Overpass |
| 7 | 1202 | I-84 | Bethel<br>Old Hawleyville Road Overpass |
| 8 | 1203 | I-84 | Brookfield<br>Secor Road Overpass |
| 9 | 1149 | I-84 | Southbury<br>Ichabut Road Overpass |
| 10 | 1475 | 172 | Southbury<br>Over Pomperaug River |
| 11 | 1047 | 67 | Southbury<br>Over Pomperaug River |

**Table I** : Description of the Location of the Initial Eleven Sites

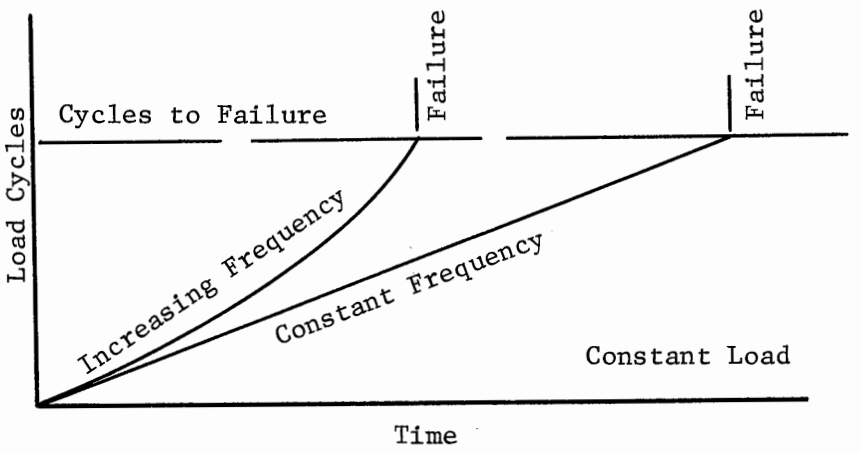


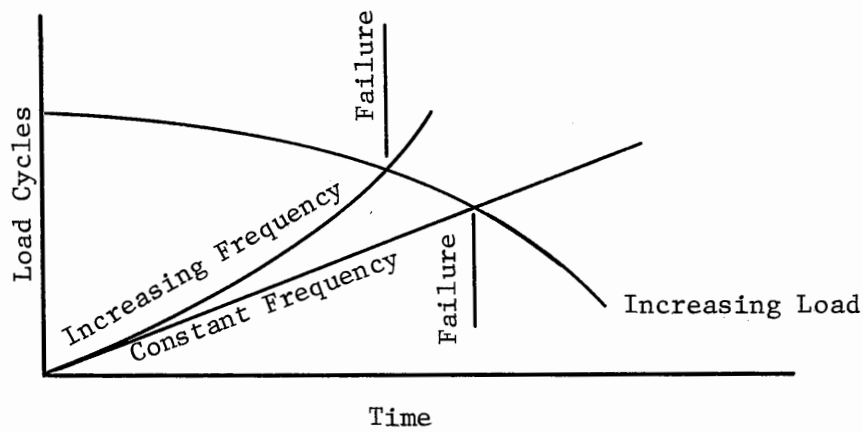


Figure 1: Time Versus Load Cycles, Fatigue

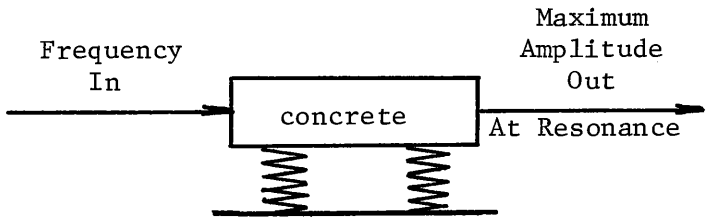


a. Laboratory Sonometer

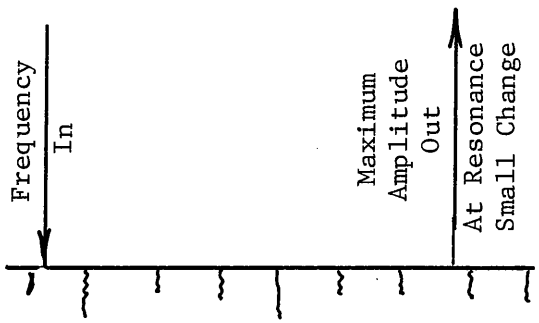


b. Field Sonometer

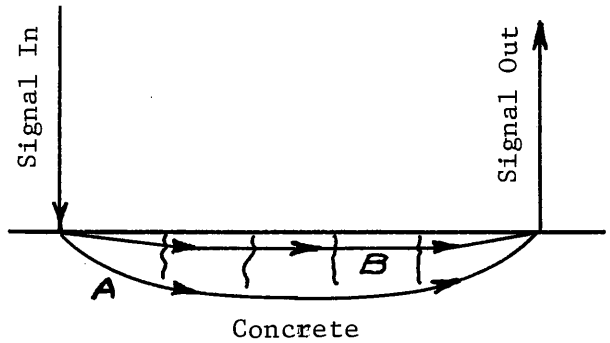


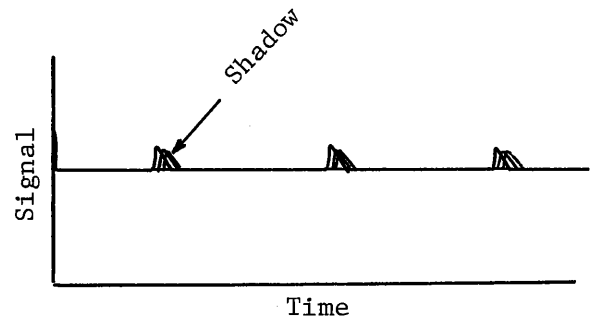


Shadow on far side due to progressively slower propagation through poor and cracked concrete. Width of shadow indicates degree of difference.

c. Seismic

Figure 2: Sound Waves in Concrete

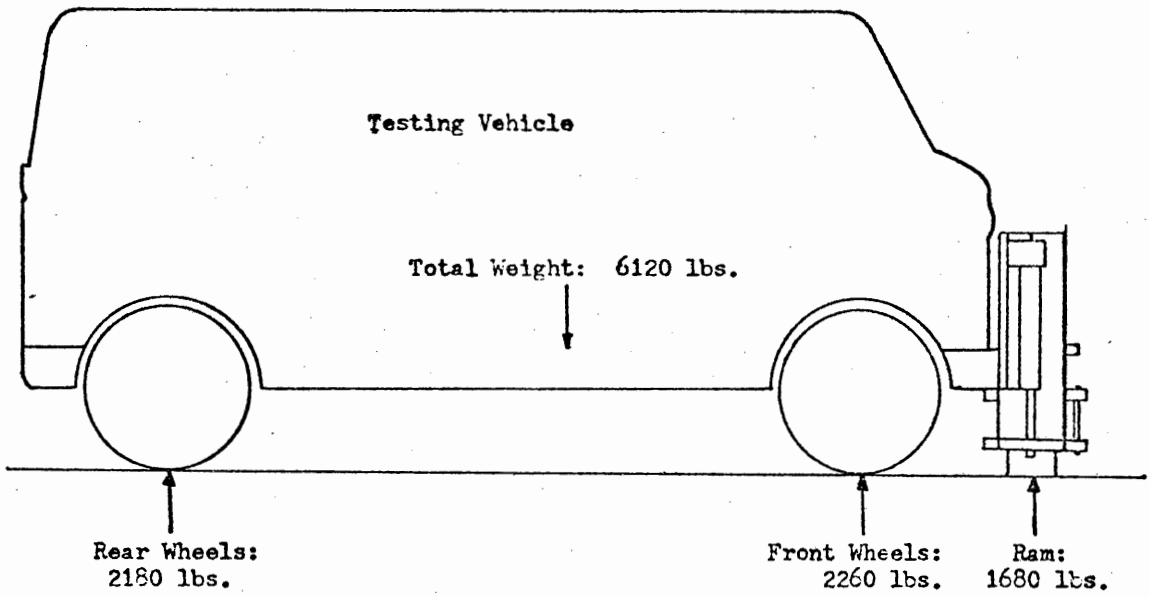


Figure a: Static Load Distribution, Ram Down and Hydraulics Pressurized 750 psi.

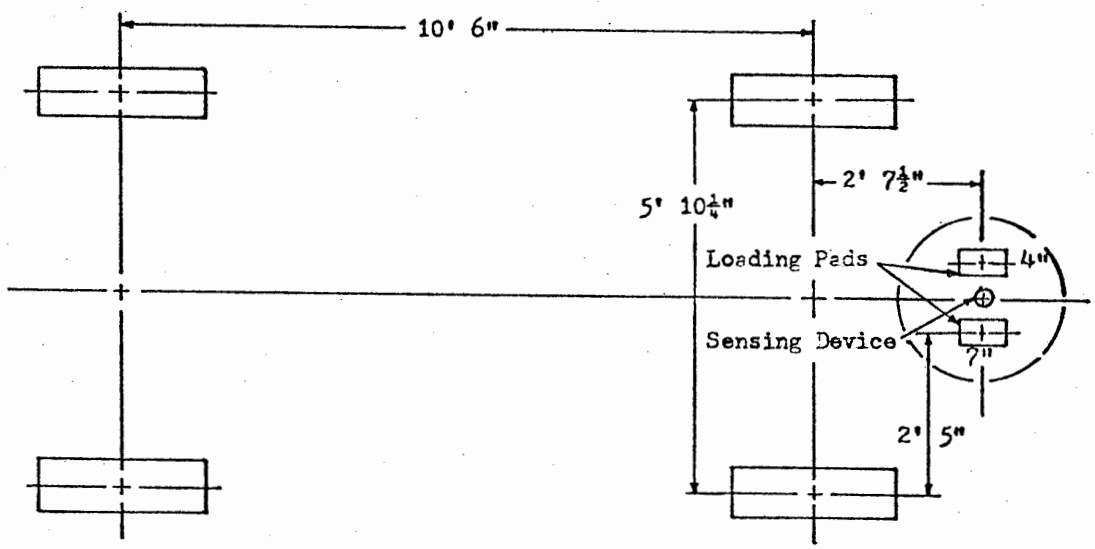


Figure b: Dimensional Configurations

Figure 3: Road Rater

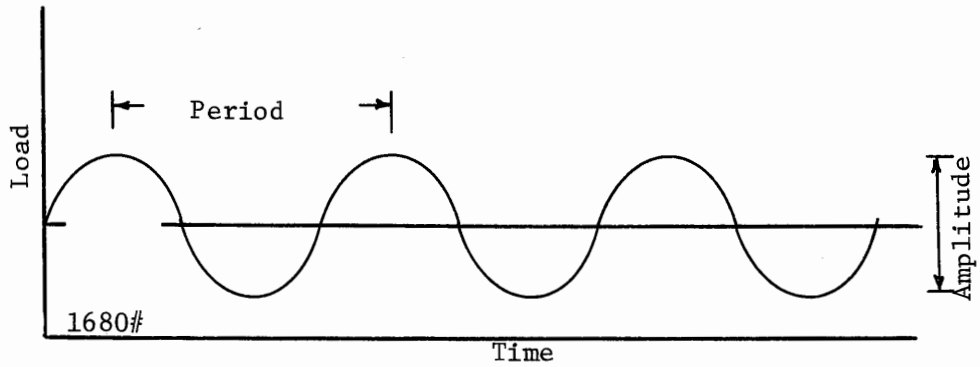


Figure 4: Road Rater Loading

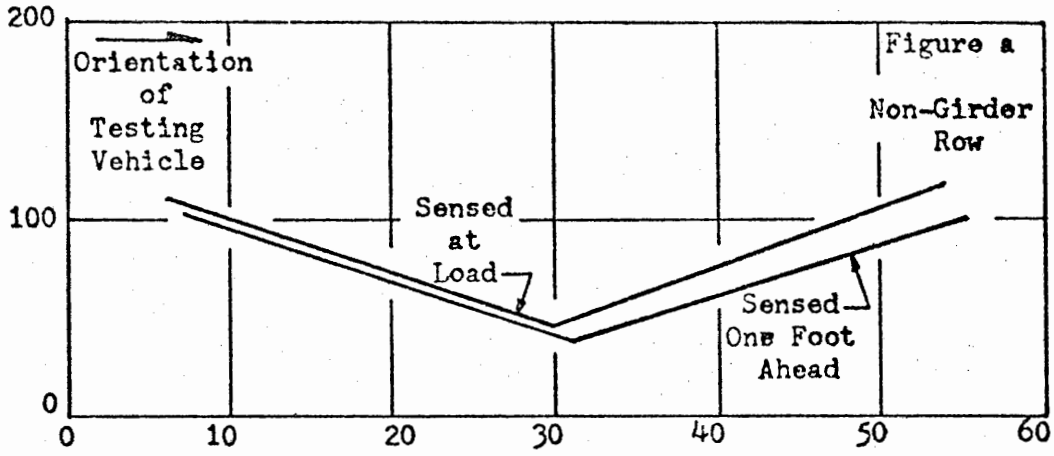


6-a: 60 Foot Interior Span of Site #7 Loaded at 6, 30, and 54' (1973)

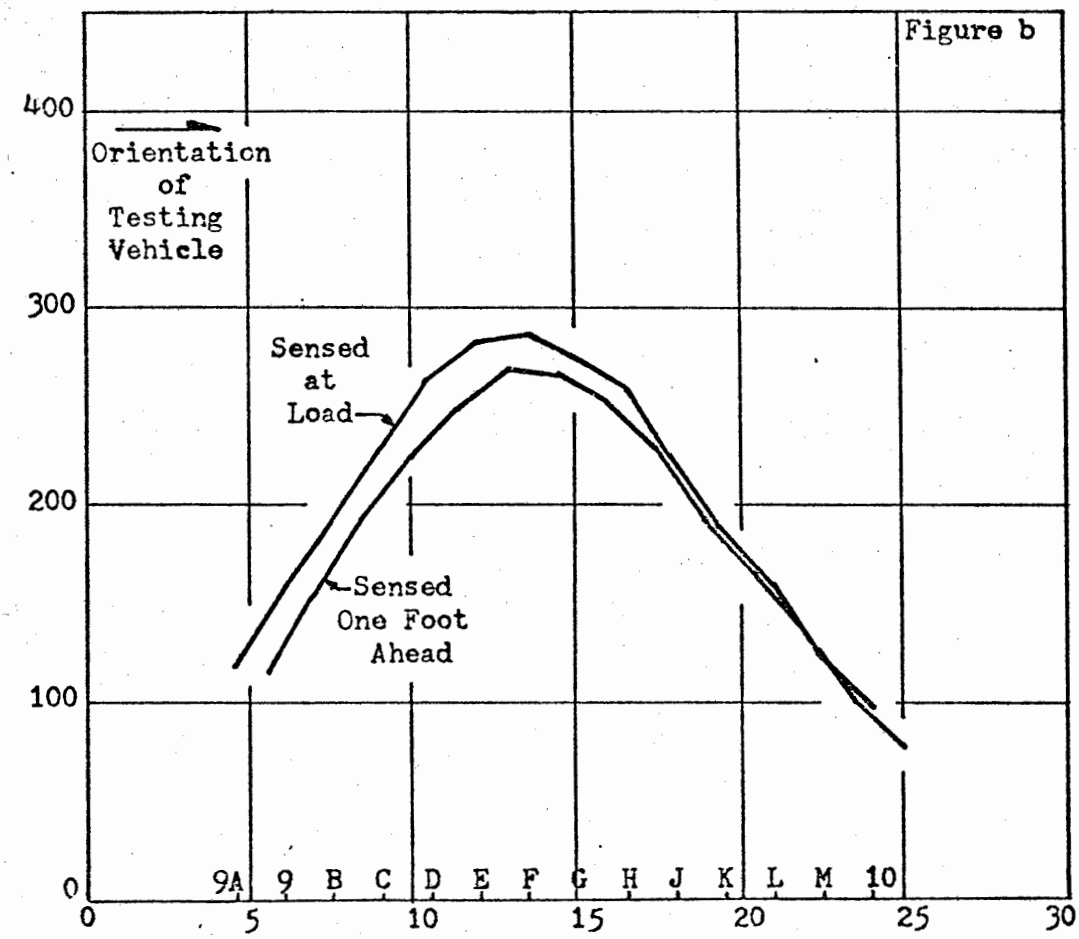


6-b: 30 Foot End Span Loaded at 1½ Foot Intervals Starting 4½ Feet From Pier End.

Figure 6: Typical Maximum Vibrational Amplitudes (1973)

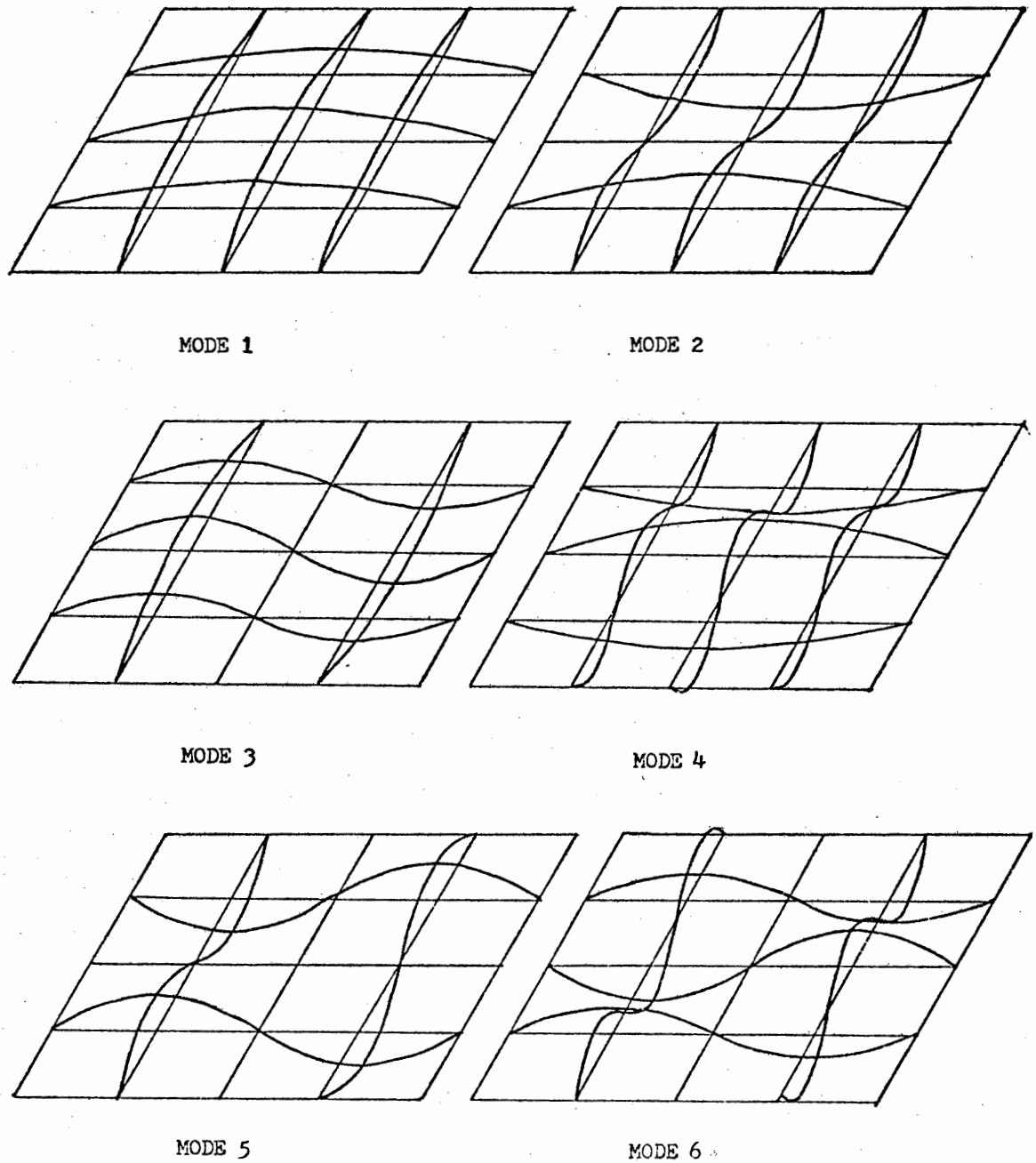


Figure 7: Low Frequency Modes of Vibration of a Simply Supported Rectangular Plate. (8)

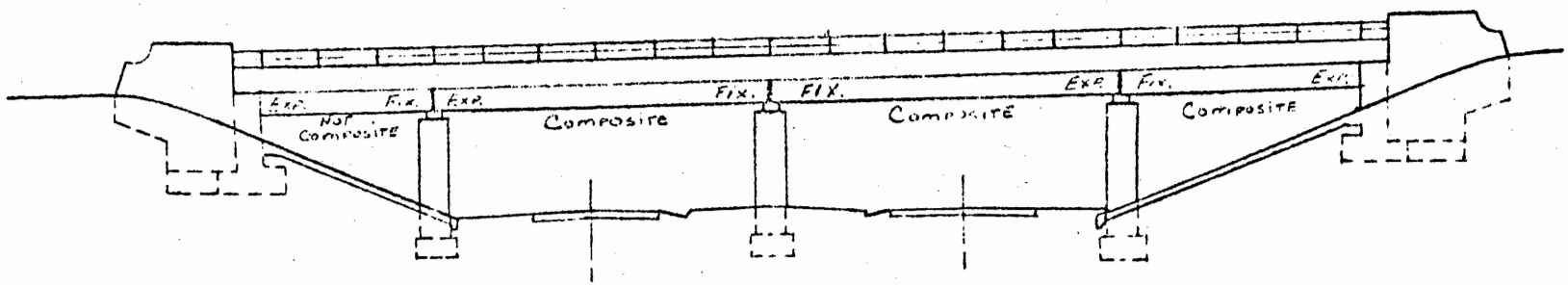


Typical Elevation View

Typical Plan View

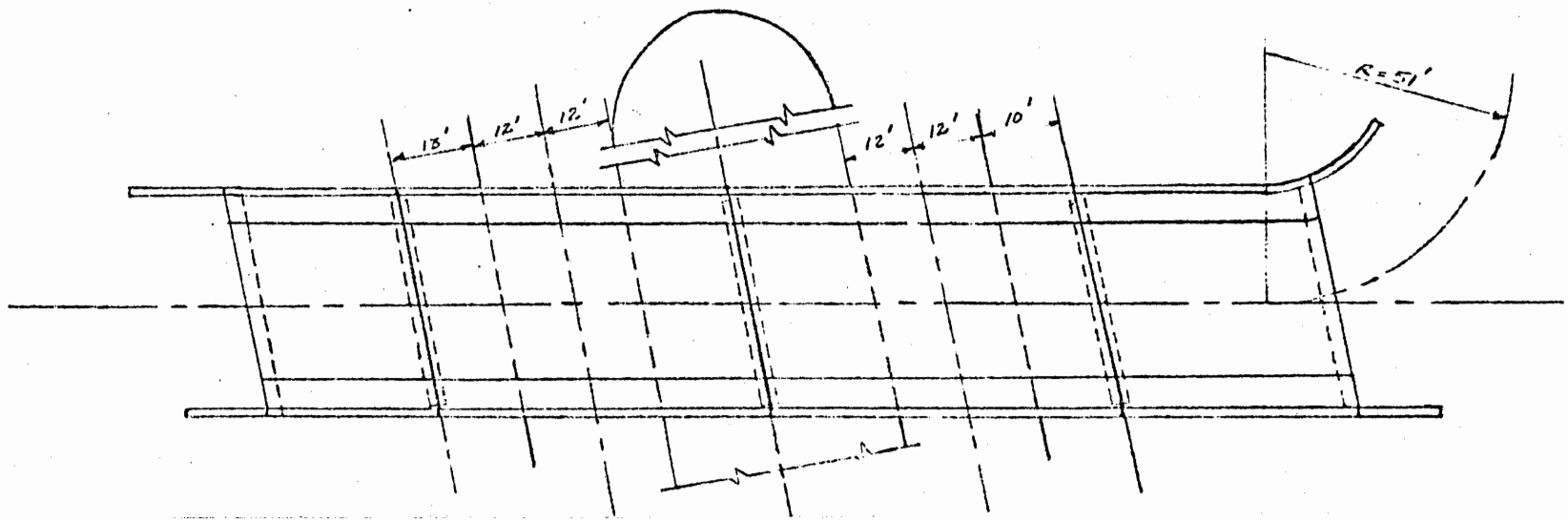


**Figure 8: Typical Plan and Elevation of Test Structures**

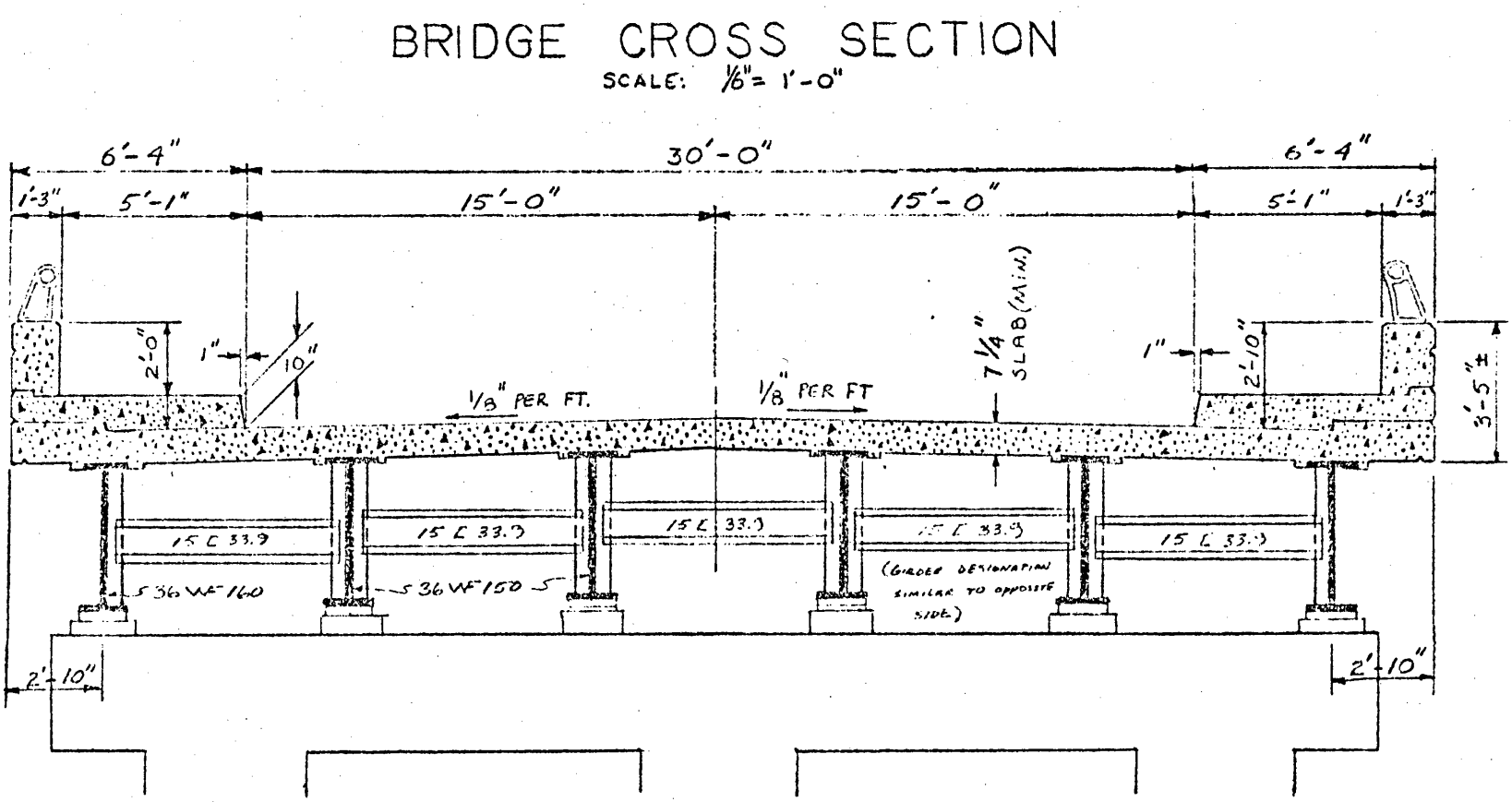


Figure 9: Typical Transverse Section of Test Structures

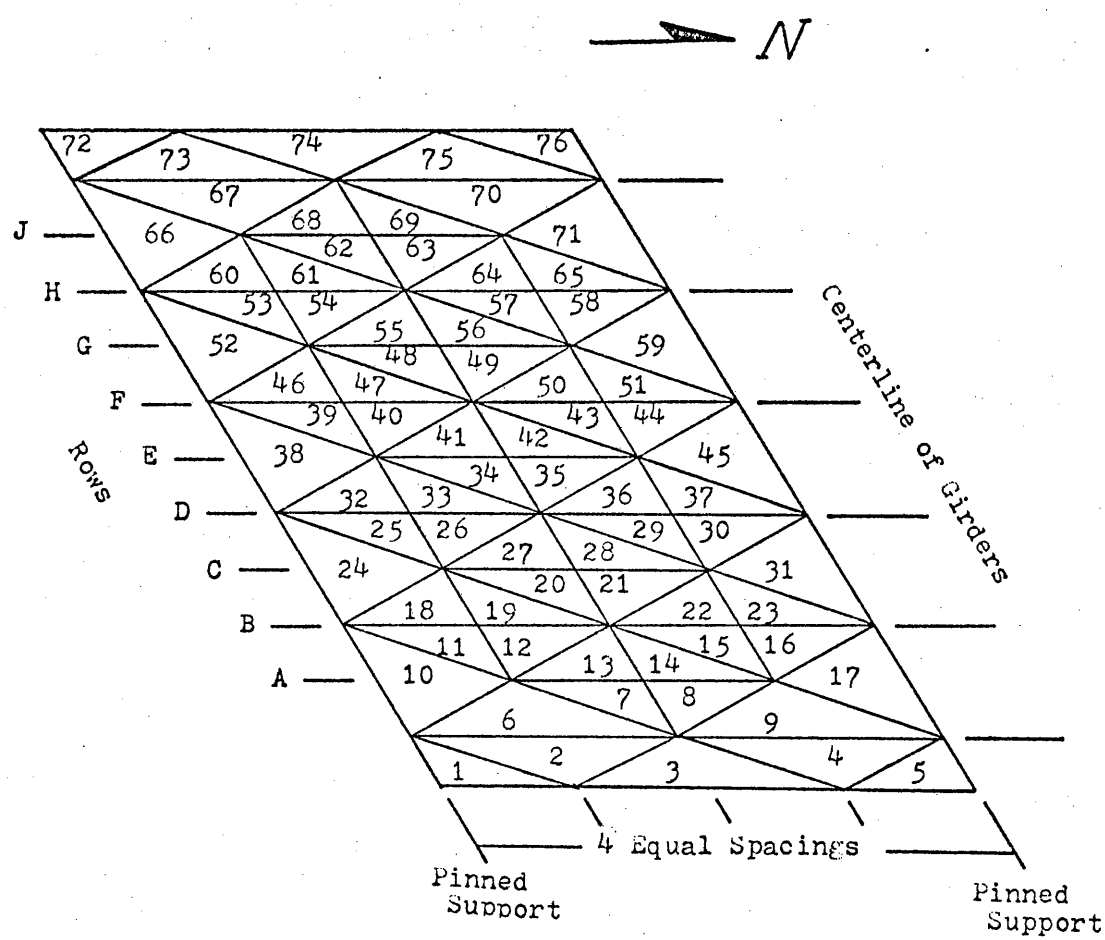


Figure 10: Layout of Finite Elements For End Spans

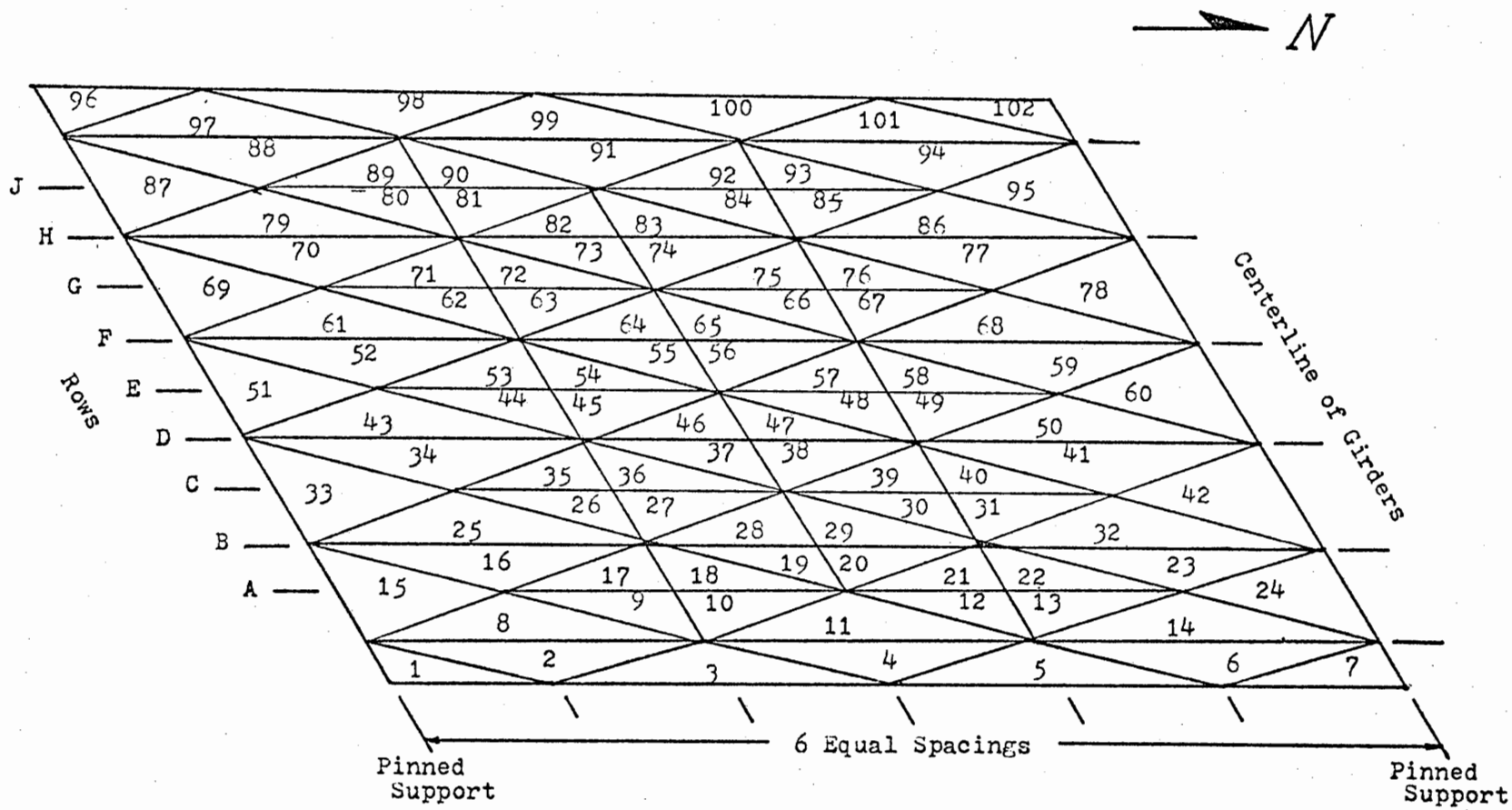


Figure 11: Layout of Finite Elements For Interior Spans, Sites #6 and #7

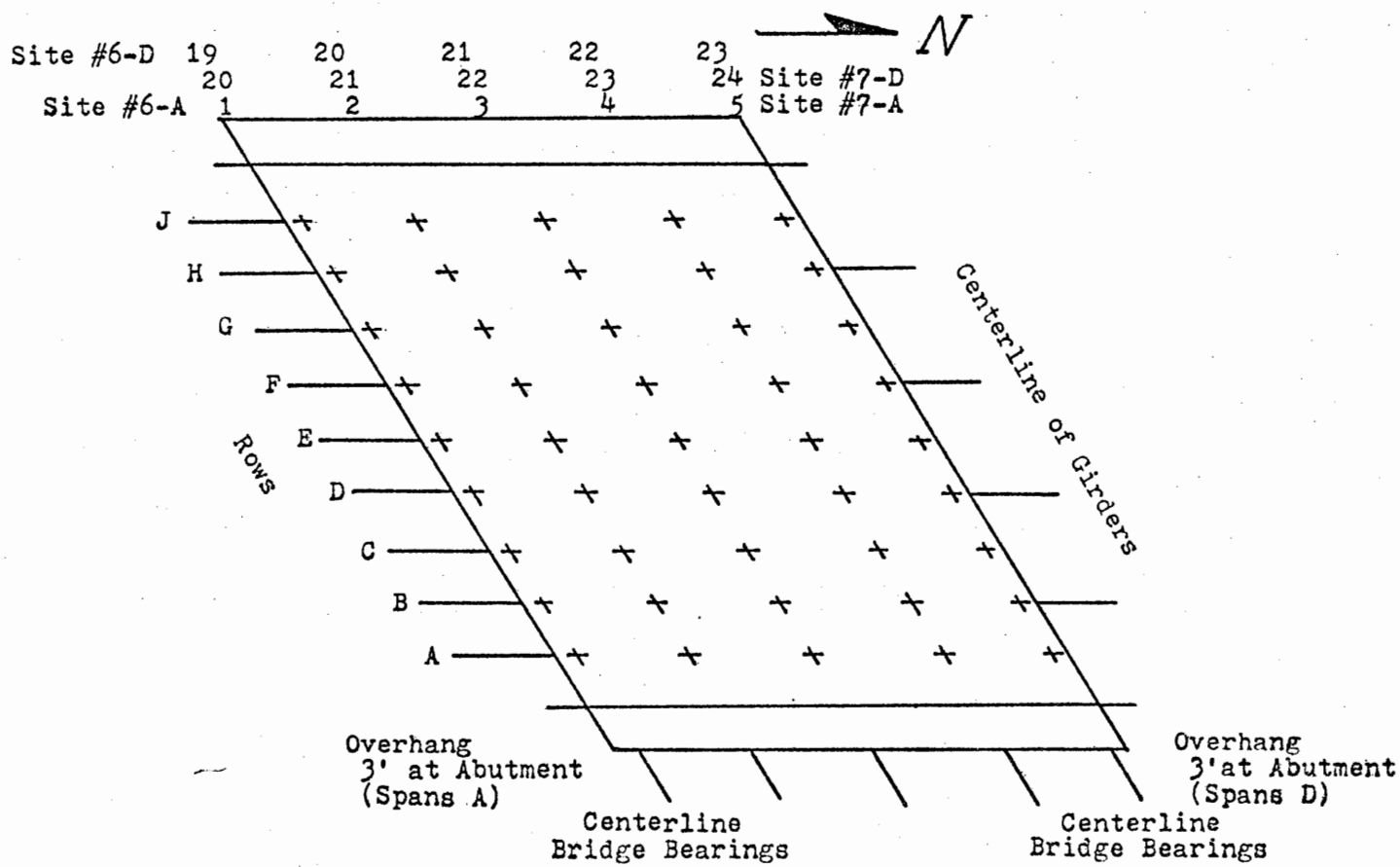


Figure 12: Test Pattern Layout, End Spans

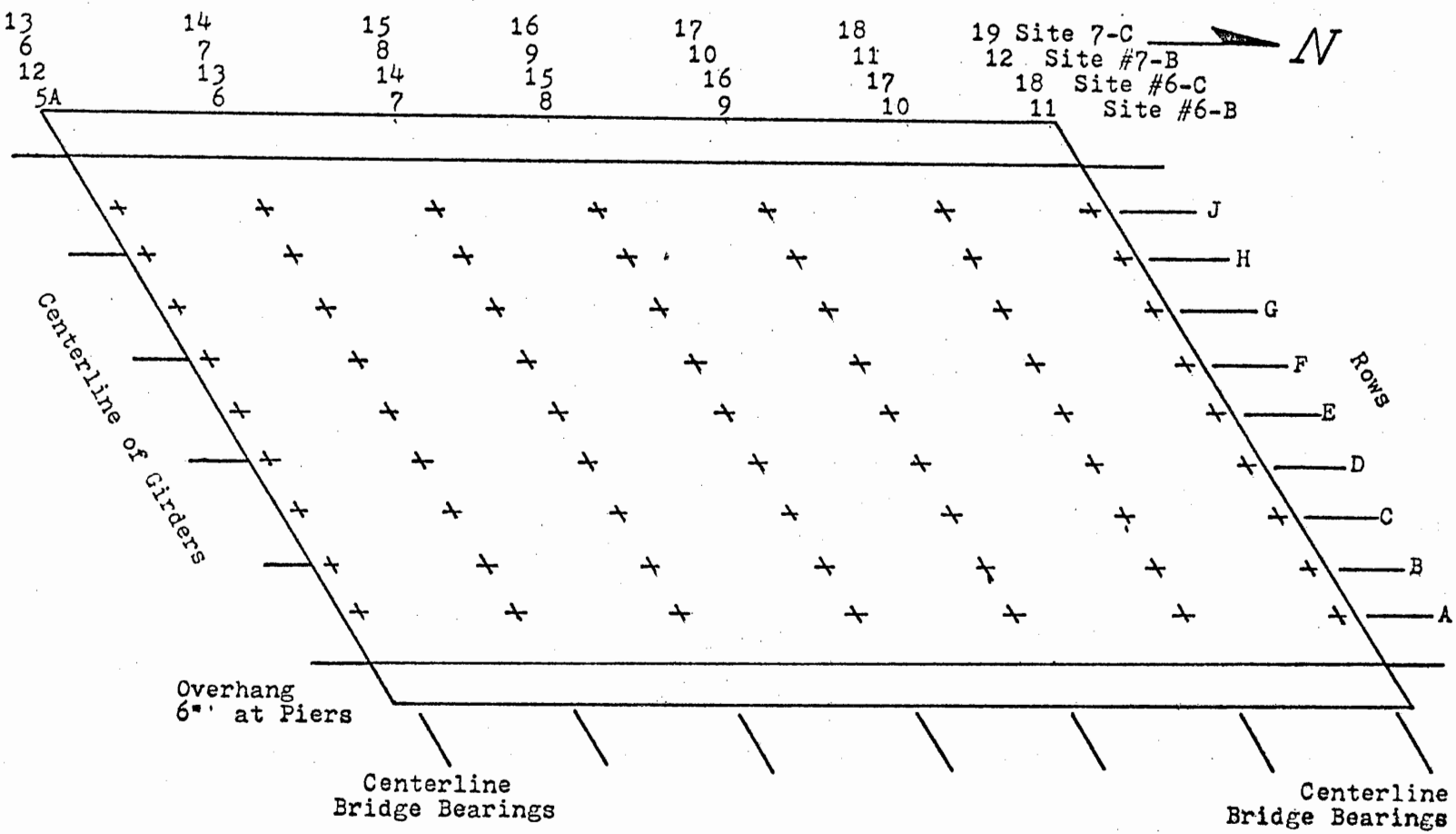


Figure 13: Test Pattern Layout, Interior Spans, Sites #6 and #7

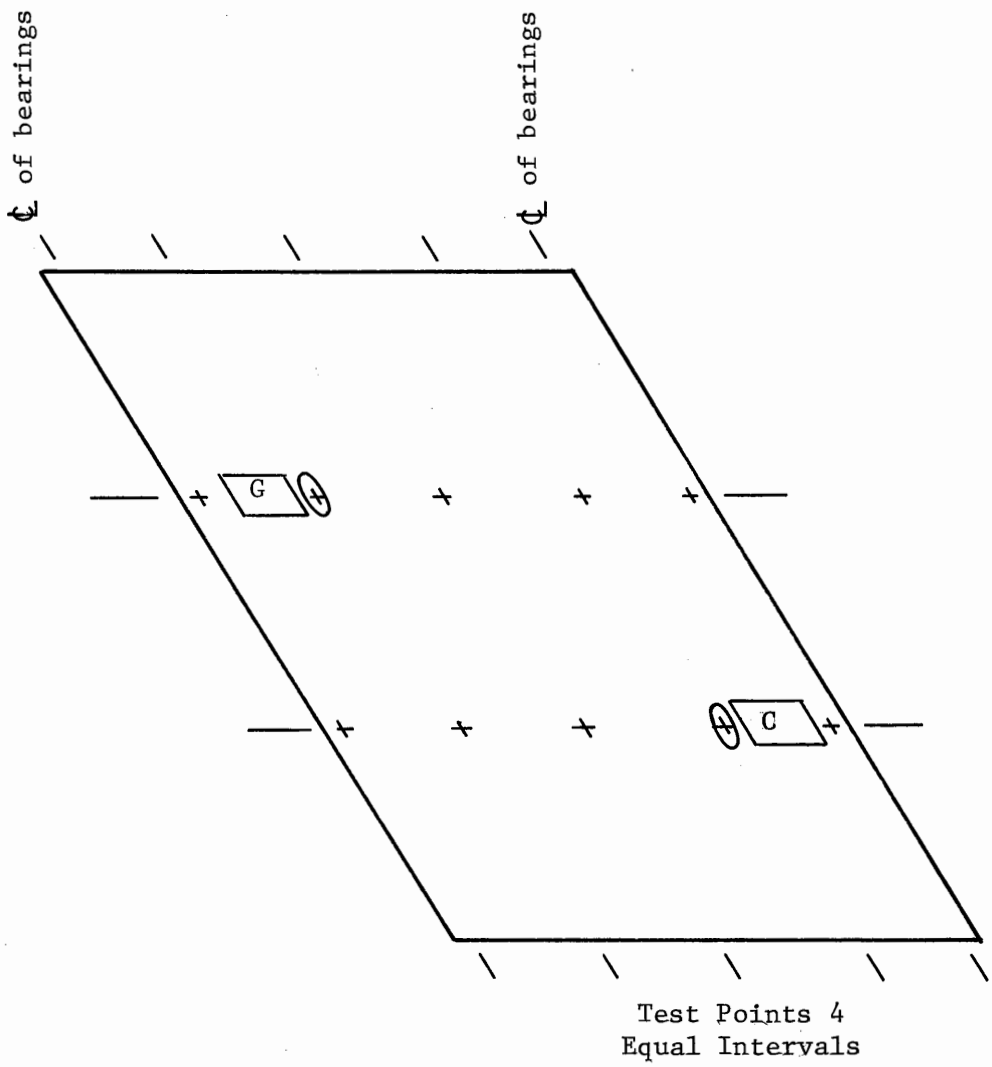


Figure 14: Symmetry of Load-Measurement Configurations

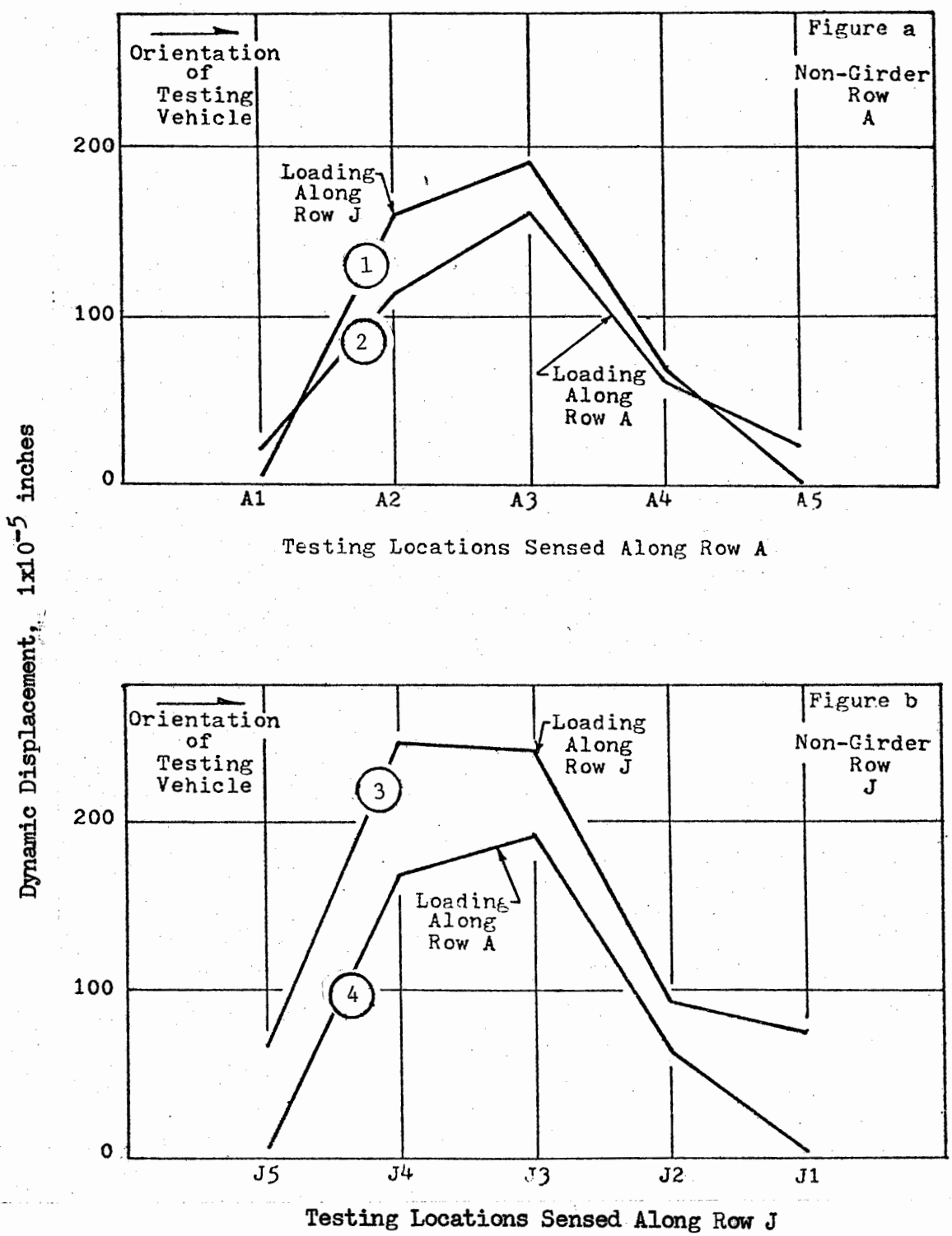


Figure 15: Amplitude Curves for End Span A, Site #7

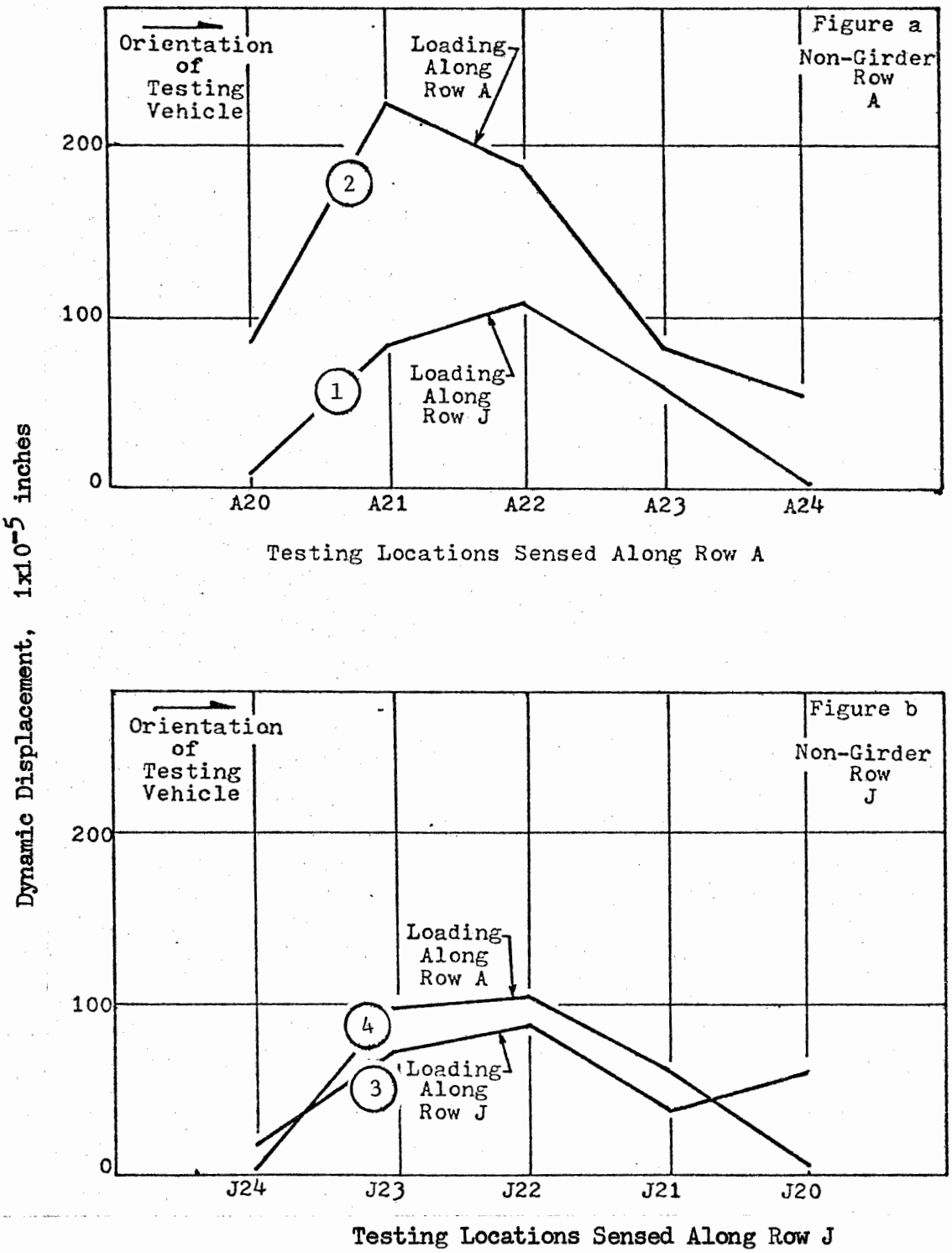


Figure 16: Amplitude Curves for End Span D, Site #7

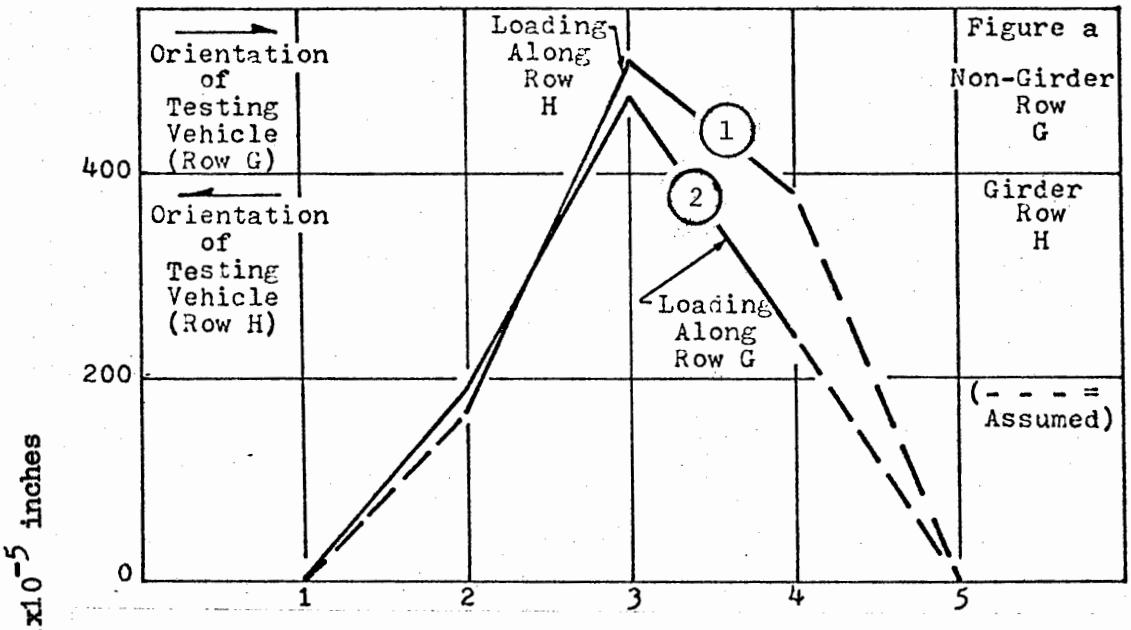


a: Amplitude Curves for End Span A, Site #7

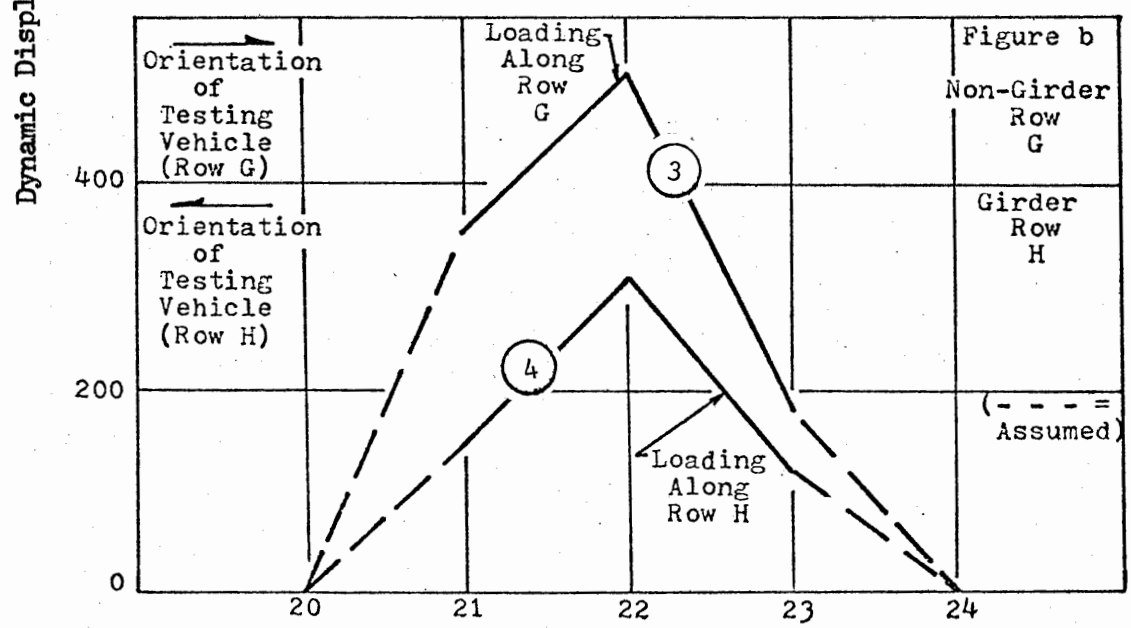


b: Amplitude Curves for End Span D, Site #7

Figure 17: Amplitude Curves for End Spans, Site #7

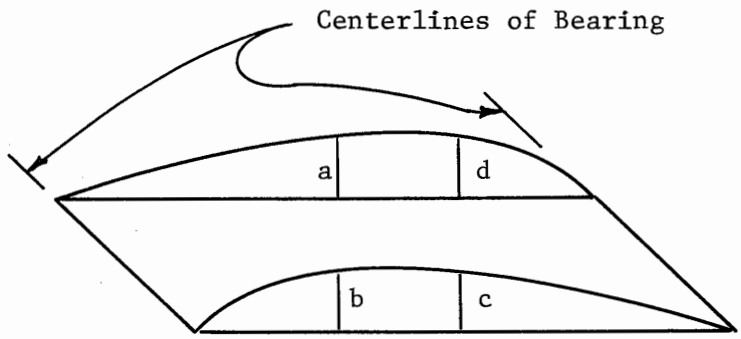


Figure 18: Skew Structure Deflections

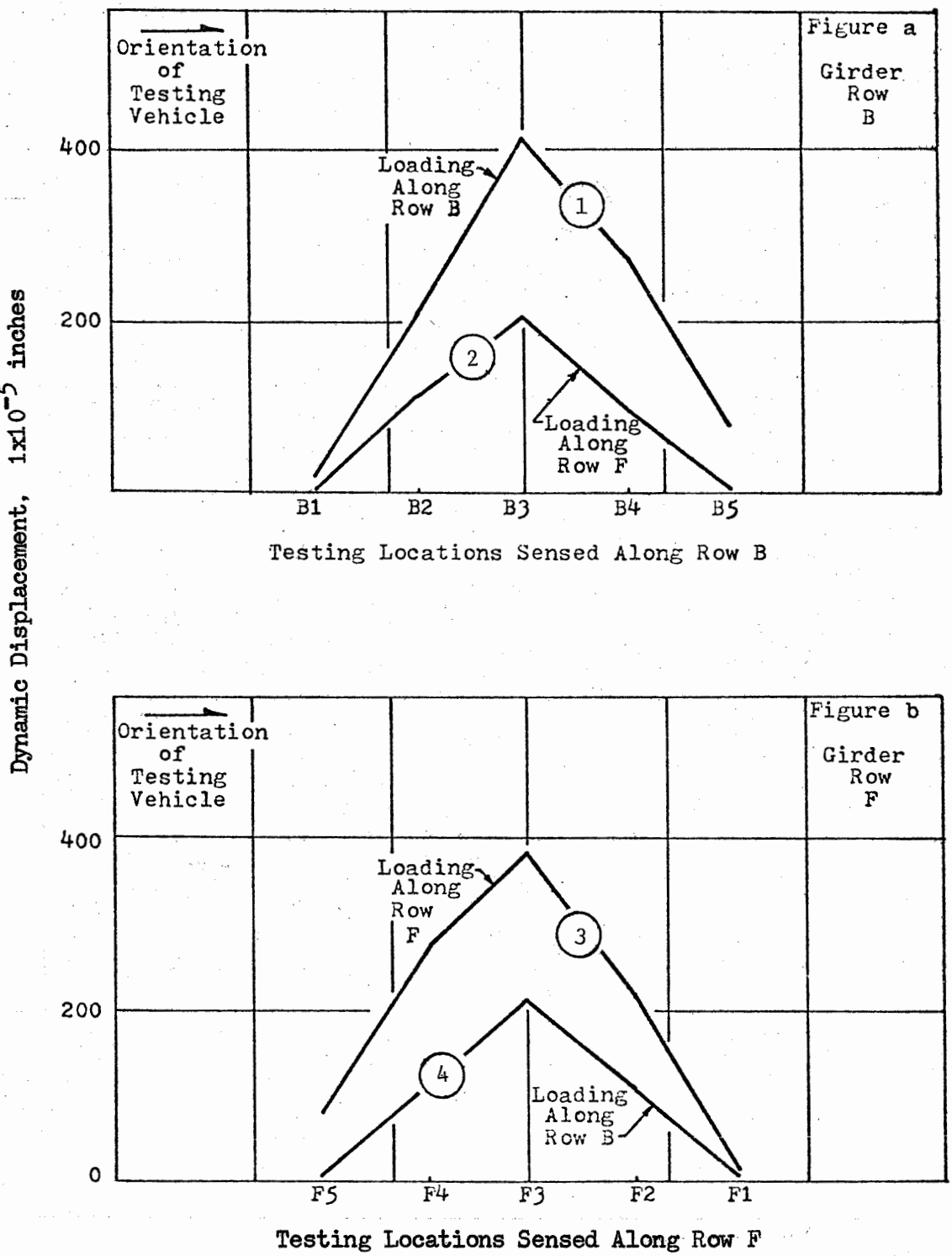


**Figure 19: Amplitude Curves doe End Span A, Site #6**

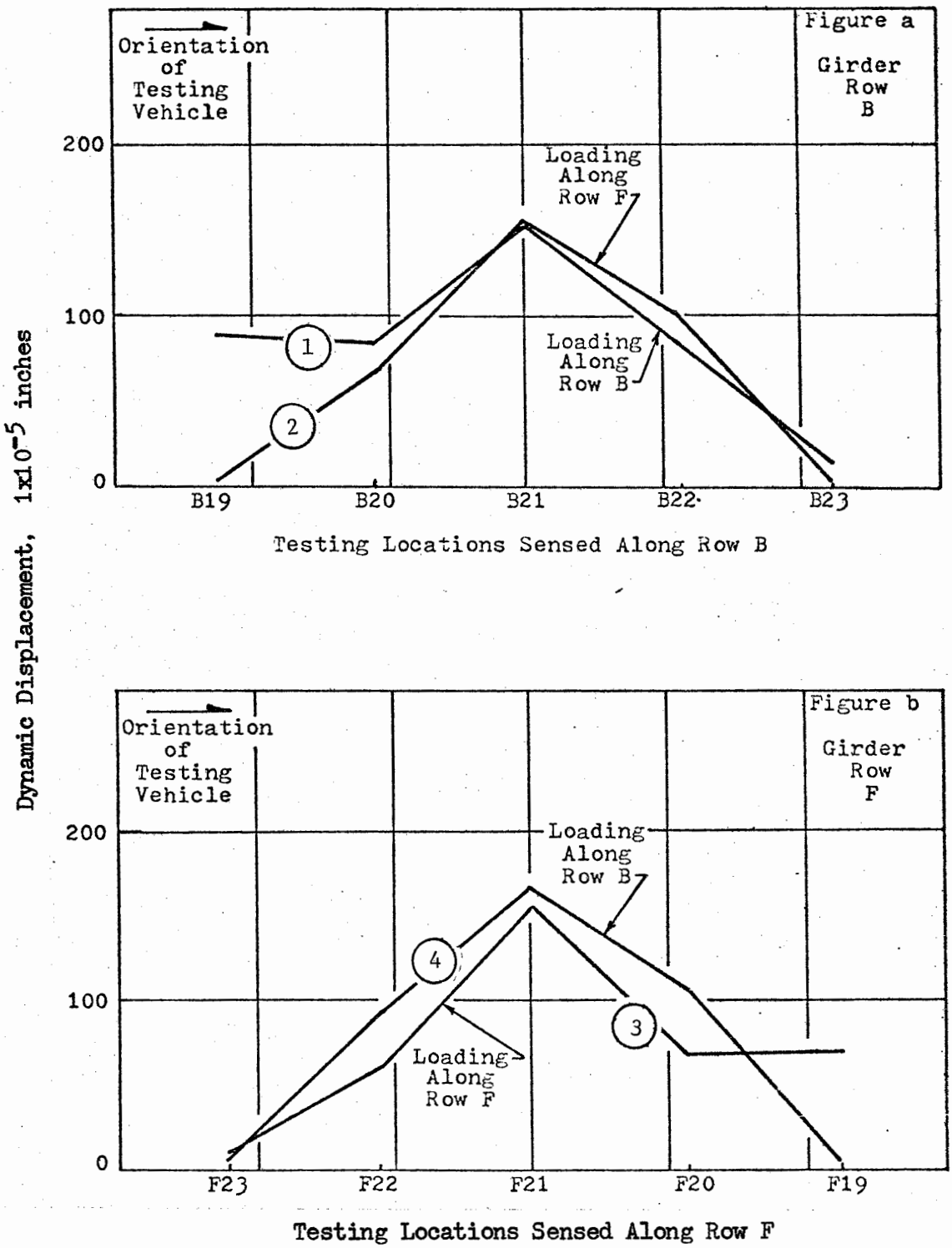


Figure 20: Amplitude Curves for End Span D, Site #6

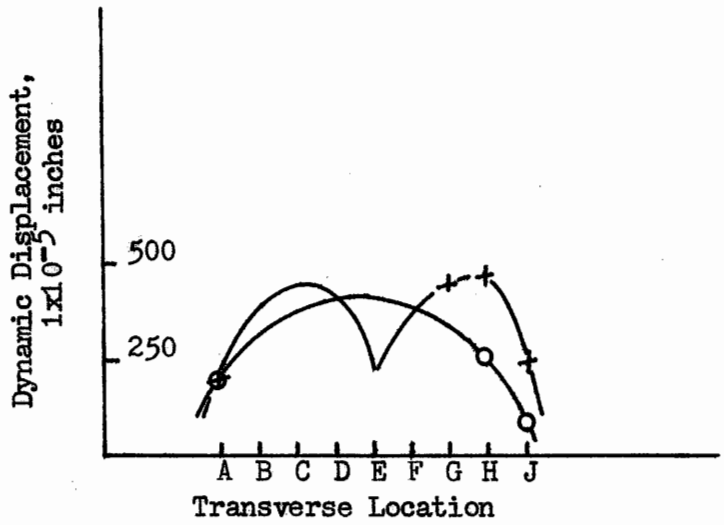


Figure 21: Cross Vibration

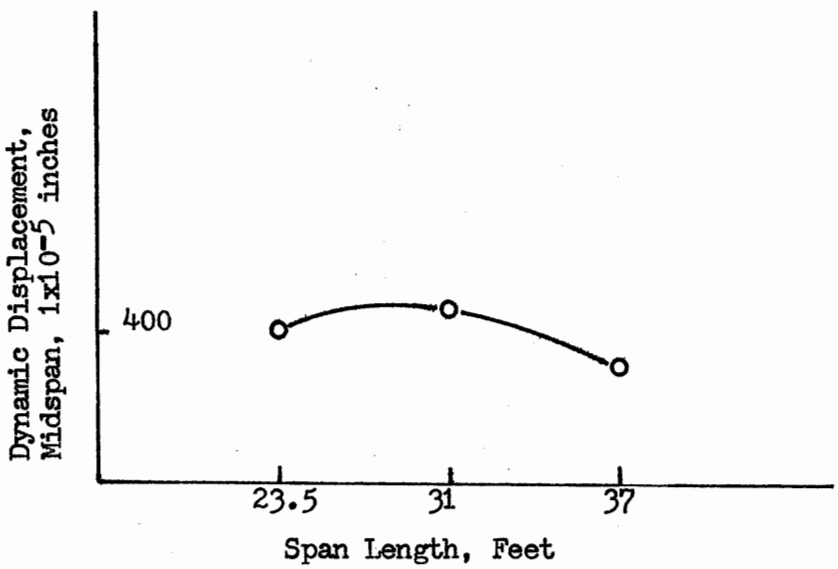


Figure 22: Length Versus Amplitude of Dynamic Displacement, Midspan.

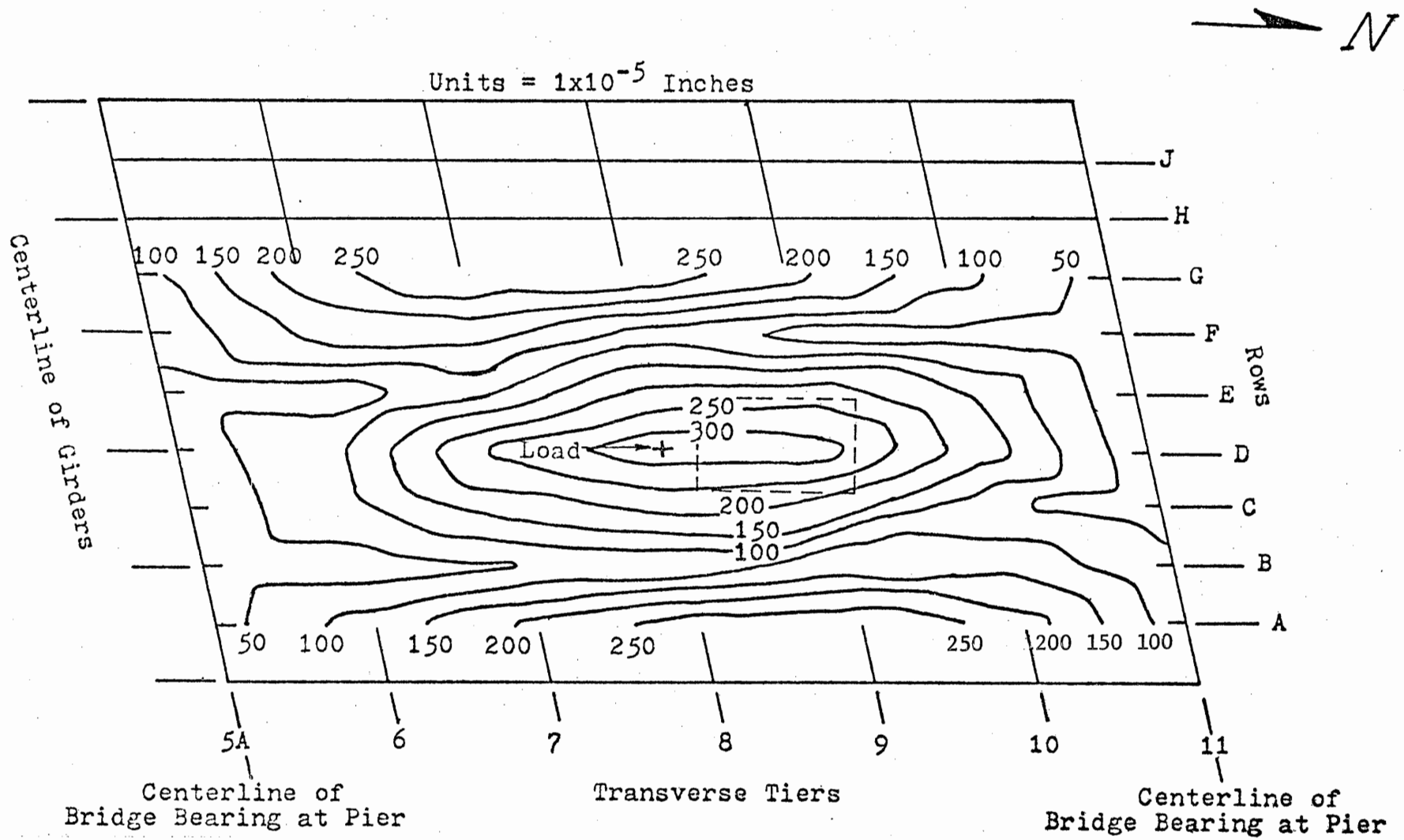


**Figure 23:** Experimental Ampligraphic Chart of Span B, Site #6, Loading D-8

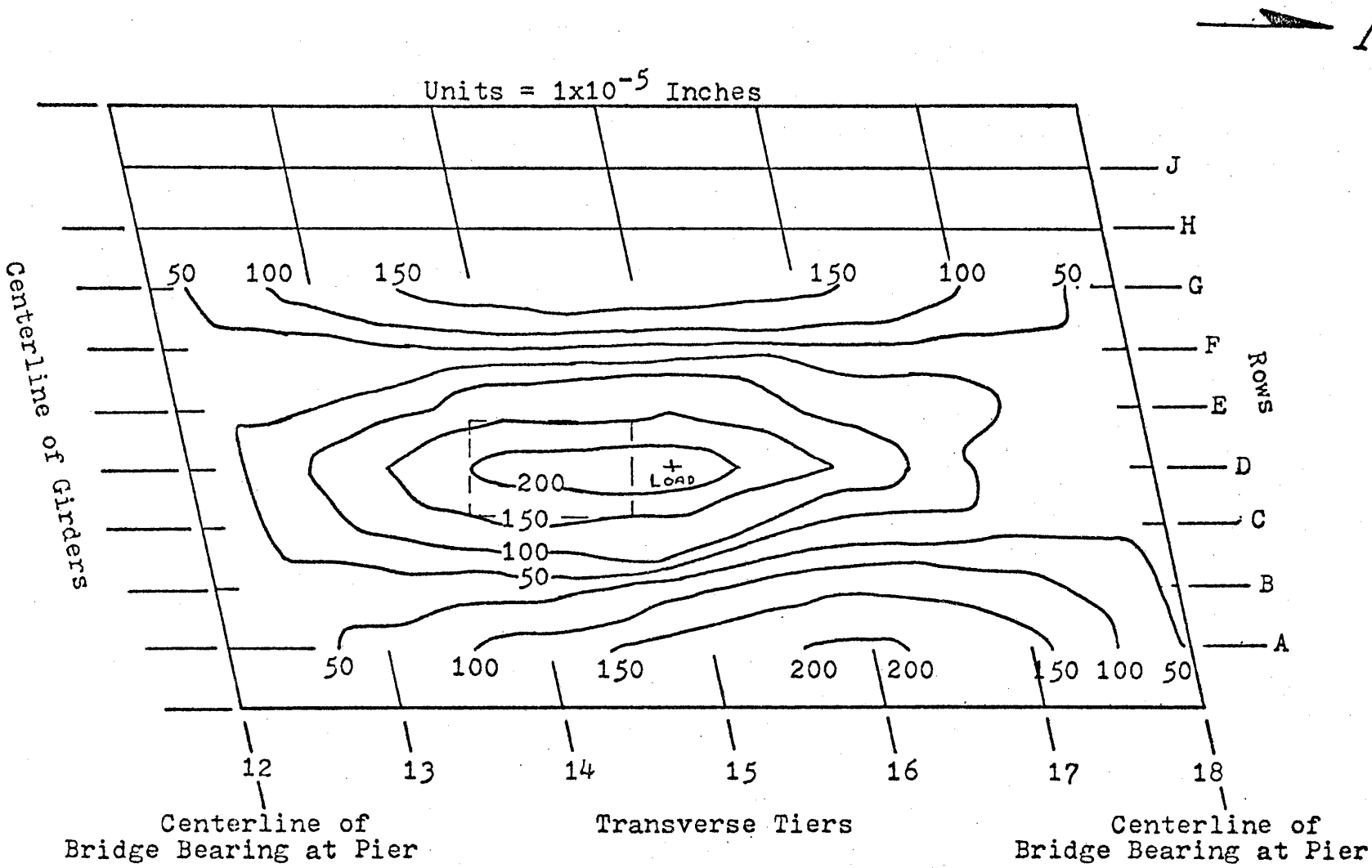


**Figure 24:** Experimental ampligraphic Chart of Span C, Site #6, Loading at D-15

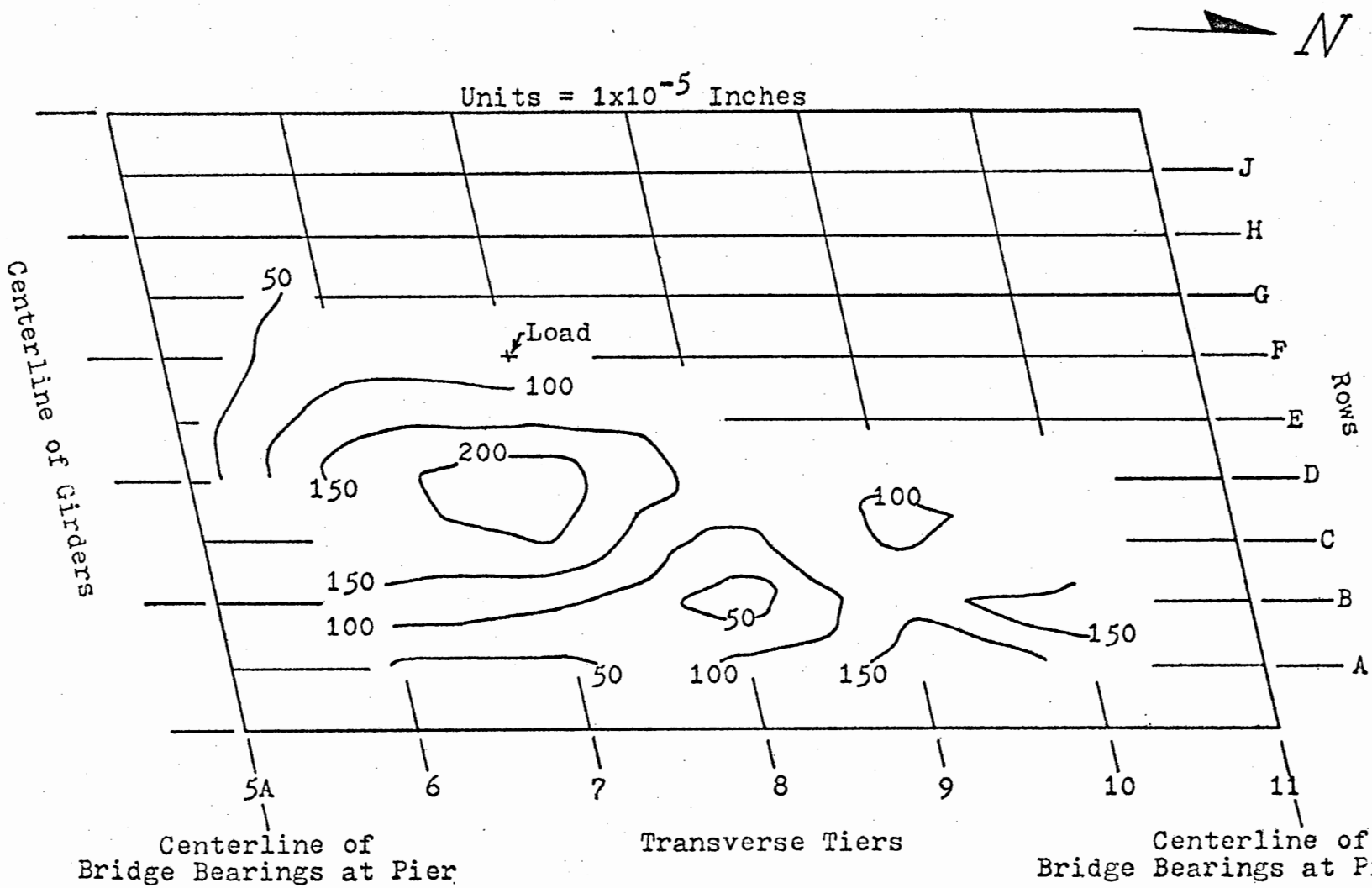


**Figure 25:** Experimental Ampligraphic Chart, Span B, Site #6, Loading at F-7

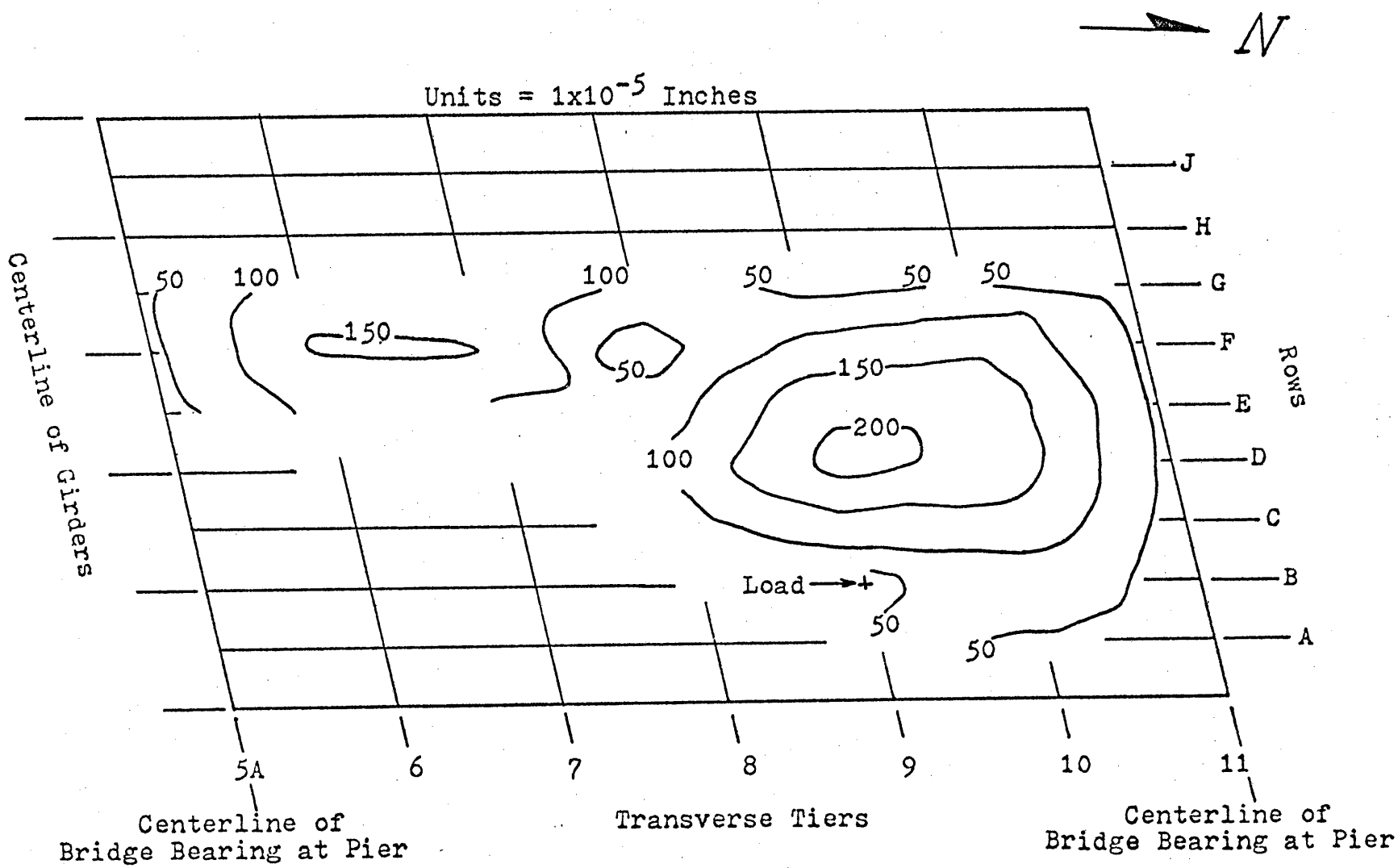


**Figure 26:** Experimental Ampligraphic Chart of Span B, Site #6, Loading at B-9

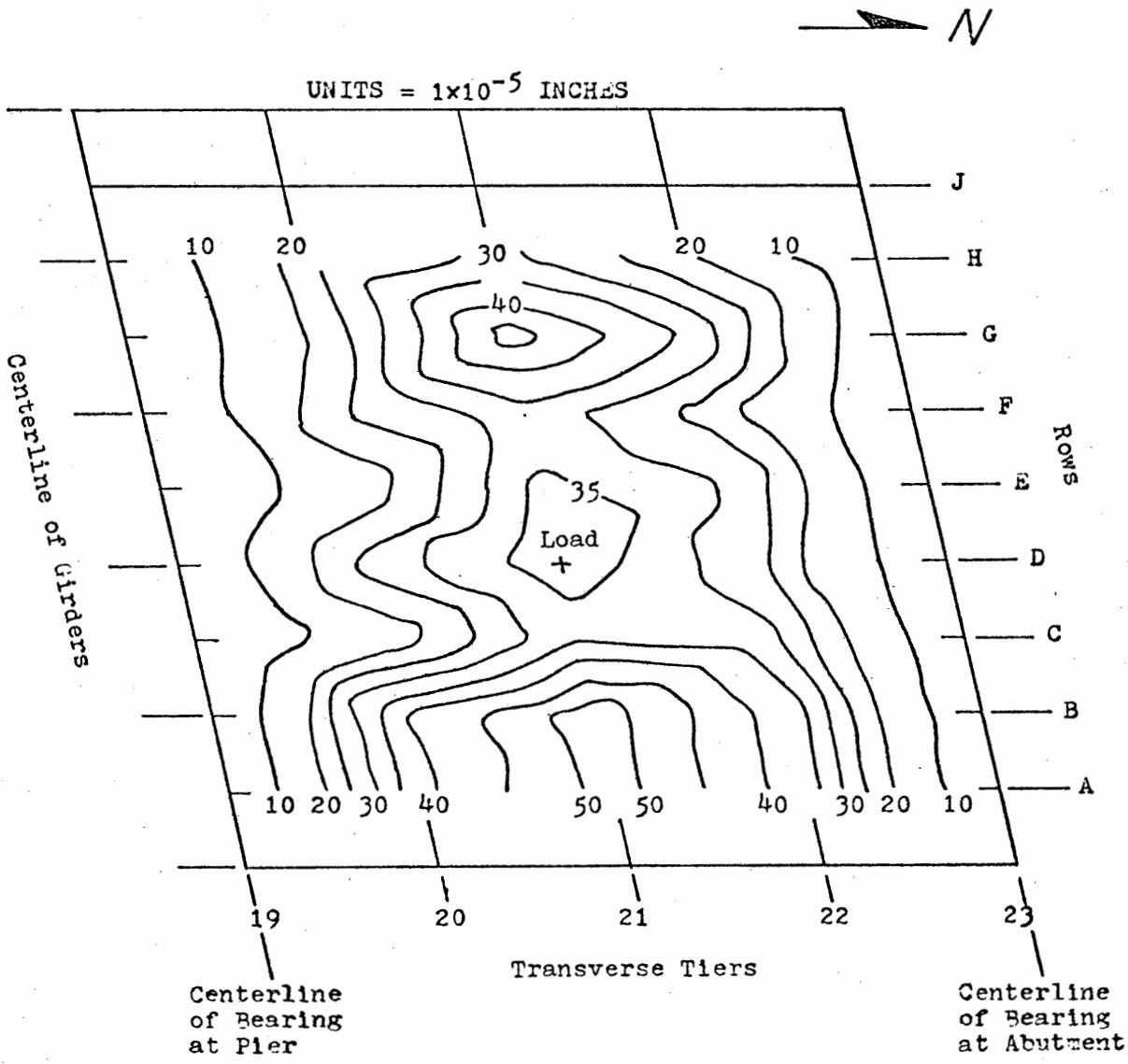


Figure 28: Chart of Computed Amplitudes for Span D, Site #6, Loaded at D-21.

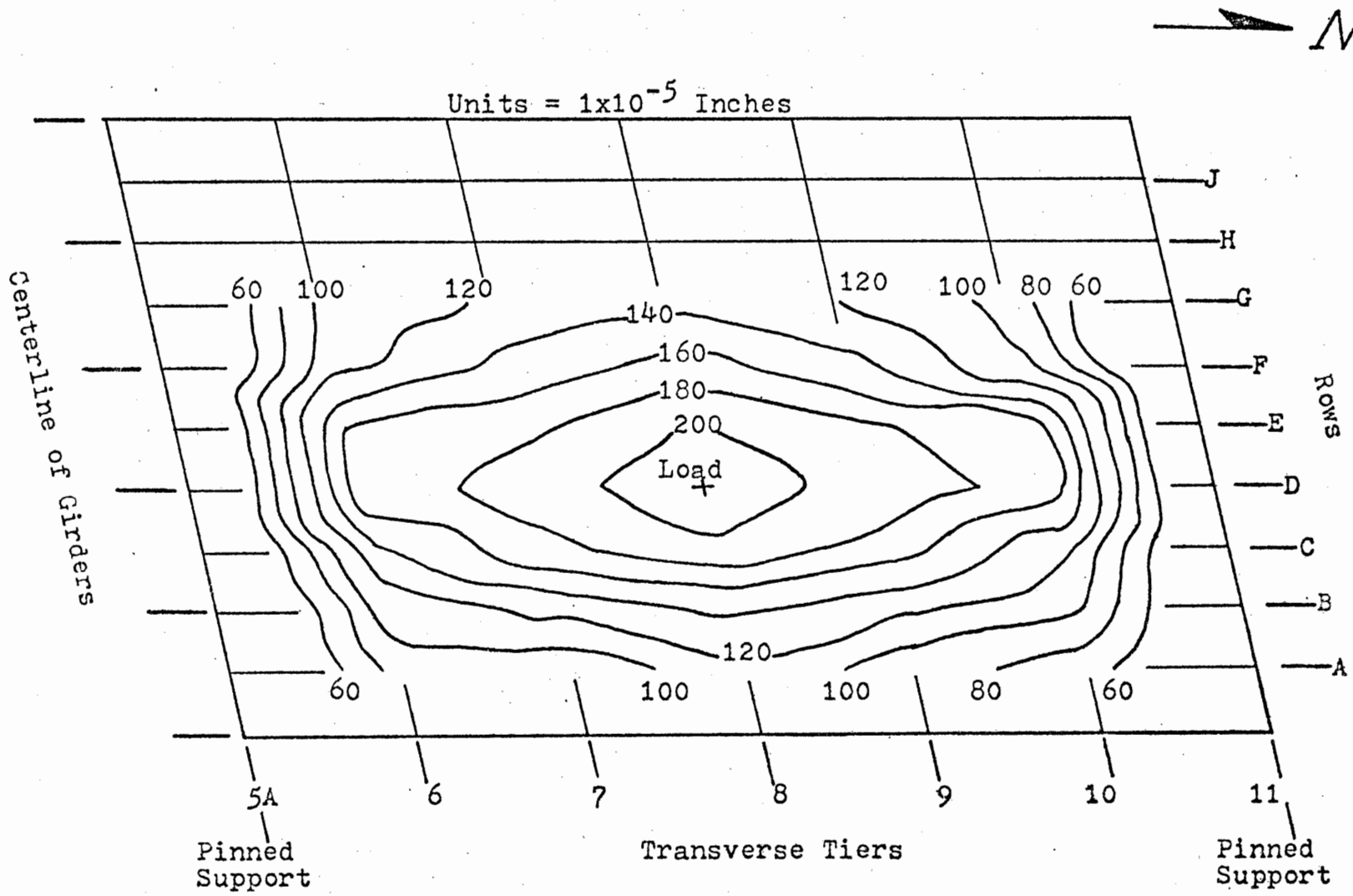


Figure 29: Chart of Computed Amplitudes for Span B, Site #6, Loaded at D-8.

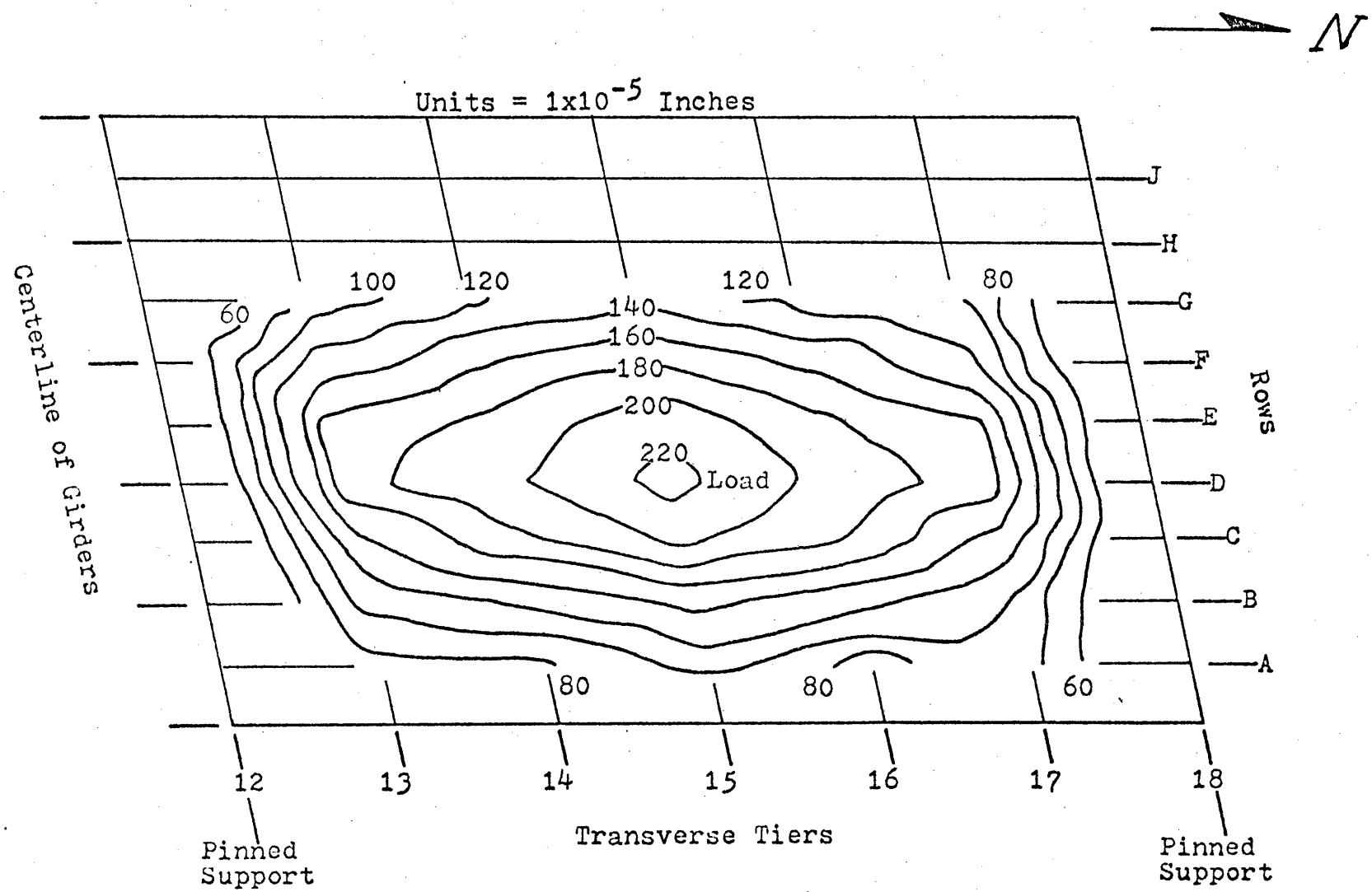


Figure 30: Chart of Computed Amplitudes for Span C, Site #6, Loaded at D-15.

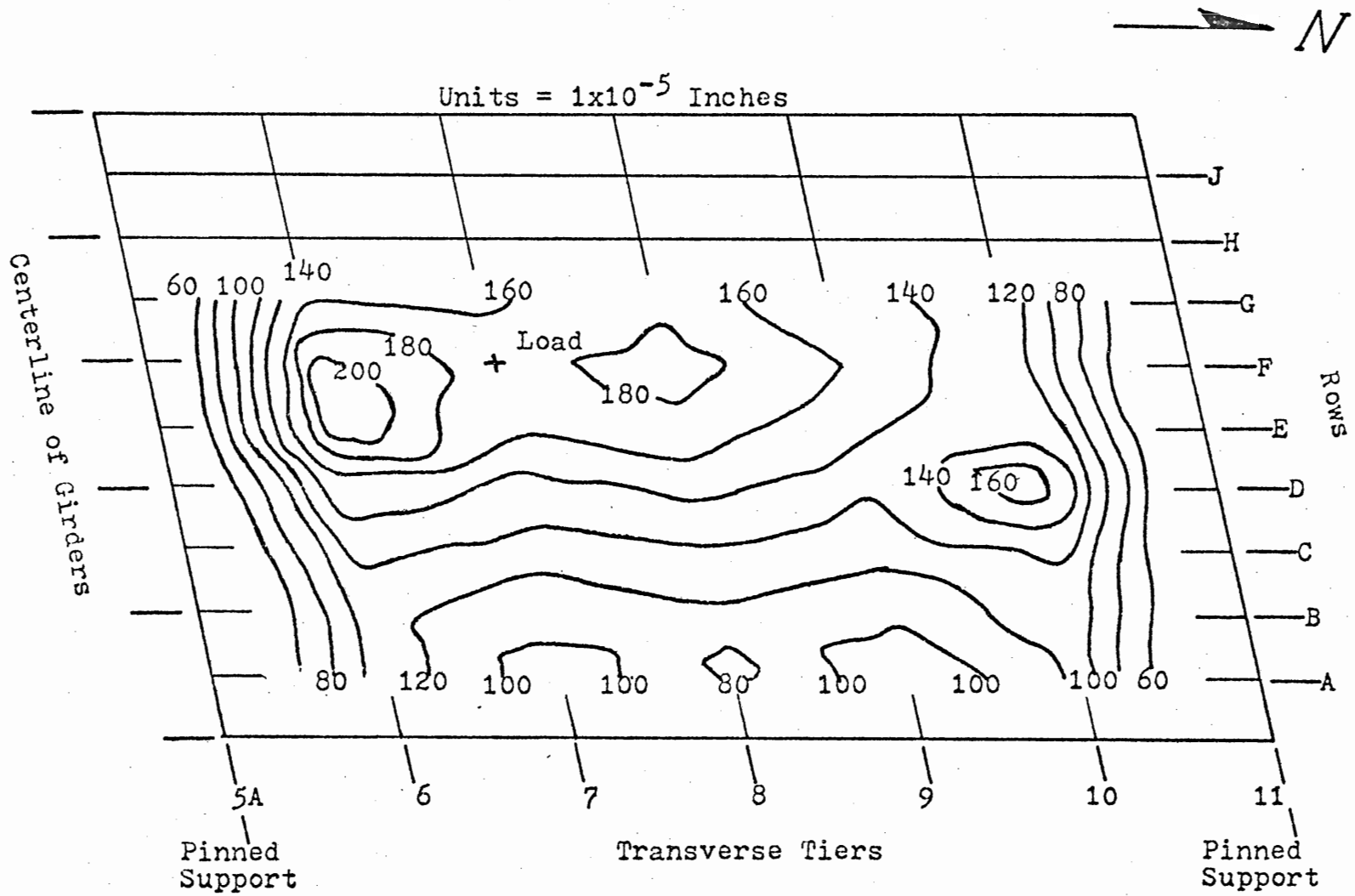


Figure 31: Chart of Computed Amplitudes for Span B, Site #6, Loaded at F-7.

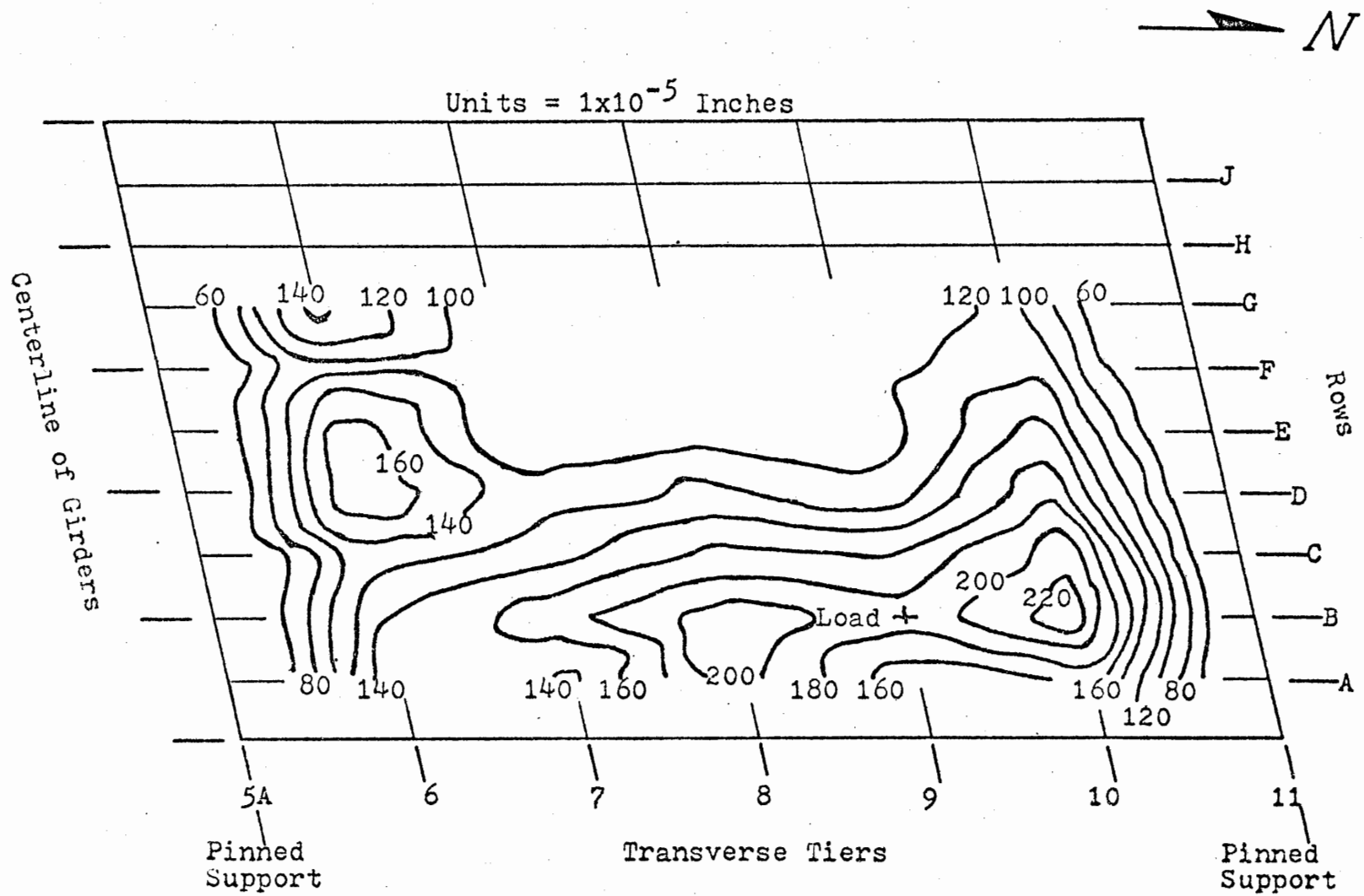


Figure 32: Chart of Computed Amplitudes for Span B, Site #6, Loaded at B-9.